

© 2024

Joshua Alan Davis

ALL RIGHTS RESERVED

ELECTROCHEMICAL MONITORING OF CORROSIVE MICROBIOLOGICAL
ACTIVITIES USING SPLIT-CELL ZERO RESISTANCE AMMETRY

A Dissertation

Presented to

The Graduate Faculty of The University of Akron

In Partial Fulfillment

of the Requirements for the Degree

Doctor of Philosophy

Joshua Alan Davis

December, 2024

ELECTROCHEMICAL MONITORING OF CORROSIVE MICROBIOLOGICAL
ACTIVITIES USING SPLIT-CELL ZERO RESISTANCE AMMETRY

Joshua Alan Davis

Dissertation

Approved:

Accepted:

Advisor
Dr. John M. Senko

Department Chair
Dr. Jordan Renna

Committee Member
Dr. Nita Sahai

Dean of the College
Dr. Mitchell S. McKinney

Committee Member
Dr. Teresa Cutright

Interim Dean of the Graduate School
Dr. Gwyneth Price

Committee Member
Dr. Lu-Kwang Ju

Date

Committee Member
Dr. Susmitha Purnima Kotu

ABSTRACT

Corrosion in natural gas transmission pipelines poses significant risks to infrastructure integrity, leading to environmental damage and economic loss. This dissertation investigates microbiologically influenced corrosion (MIC) mechanisms and develops detection methods using split-chamber zero-resistance ammetry (SC-ZRA). Microbial cultures were enriched from natural gas pipeline samples, focusing on fermentative and sulfur-metabolizing bacteria, and their corrosion activities were evaluated using SC-ZRA.

Chapter I reviewed the threat corrosion posed to carbon steel pipelines transporting oil and natural gas, emphasizing MIC's role. It described the electrochemical nature of corrosion and explained how microorganisms like sulfate-reducing and fermentative bacteria accelerated the process through biofilm formation, production of corrosive metabolites, and disruption of electrochemical balance. The chapter also highlighted electrochemical techniques, particularly SC-ZRA, used to detect and monitor MIC. ZRA allowed real-time observation of corrosion currents and distinguished between biotic and abiotic corrosion activities. Chapter II demonstrated that organic acid production by fermentative bacteria lowered pH, accelerating corrosion through cathodic hydrogen reduction on carbon steel. When buffered with sodium bicarbonate, acidity was reduced, effectively mitigating corrosion. Chapter III explored sulfur-metabolizing bacteria's role in corrosion. Experiments with thiosulfate and thiols showed that these

bacteria, particularly *Desulfovibrio alaskensis*, produced sulfide, promoting corrosion. SC-ZRA measurements highlighted how cysteine degradation and thiosulfate reduction drove electron transfer, leading to metal oxidation. Metagenomic analysis confirmed the presence of genes responsible for sulfate and thiosulfate reduction and hydrogenase activity, indicating that diverse metabolic pathways contributed to corrosion. Chapter IV discussed the integration of microbiology and electrochemistry to uncover the mechanisms of MIC in oil and gas systems. It highlighted how organic acid production by fermentative bacteria lowered pH, driving localized corrosion on carbon steel, while sulfur-reducing bacteria metabolized thiosulfate and thiols, producing corrosive byproducts like sulfide. The use of SC-ZRA enabled real-time monitoring of microbial activities and electrochemical changes, linking metabolic pathways to corrosion processes. Metagenomic analysis identified key genes driving these activities, leading to mitigation strategies like buffers, biocides, enzyme inhibitors, and sulfur-binding agents to protect infrastructure.

DEDICATION

This journey has been a collective effort, and I owe my gratitude to many. To my family, whose unwavering support and belief in me provided the foundation I needed to persevere. To the faculty and advisors who shared their wisdom, challenged my thinking, and guided me through the complexities of research. To my friends, who offered camaraderie and understanding, reminding me to find balance amidst the demands of academia. Each of you has played a crucial role in my journey, and I thank you all for your contributions. This work is as much yours as it is mine.

ACKNOWLEDGEMENT

We express our sincere gratitude to Rick Eckert, Chris Kagarise, and Susmitha Kotu from DNV for their assistance in obtaining the pigging sludge samples essential for this study. This research was made possible through the support of the United States Department of Transportation Pipeline and Hazardous Materials Safety Administration, under contract 693JK31850003CAAP. Their contributions have been instrumental to the progress and success of this work. Additional support for this work was from the Ohio Water Resources Center. I would also like to thank Dr. Chelsea Monty-Bromer of Cleveland State University, Dr. Sai Prasanna Chinthala and Dr. Anwar Sadek of Corrolytics, LLC for their support during the experimental process and beyond.

TABLE OF CONTENTS

	Page
LIST OF FIGURES	ix
LIST OF TABLES	xi
CHAPTER	
I. BACKGROUND.....	1
1.1. The Problem with Corrosion	1
1.2. Microbially Influenced Corrosion	1
1.3. Detecting MIC	5
1.4. Dissertation Overview	9
II. ELECTROCHEMICAL DETECTION OF CARBON STEEL CORROSION INDUCED BY FERMENTATIVE BACTERIA FROM NATURAL GAS TRANSMISSION LINES	14
2.1. Abstract.....	14
2.2. Introduction.....	15
2.3. Experimental Procedure.....	17
2.4. Results and Discussion	22
III. PATHWAYS OF CORROSION INDUCED BY THIOSULFATE REDUCING ANDTHIOL METABOLIZING BACTERIA	33
3.1. Abstract.....	33
3.2. Introduction.....	34
3.3. Experimental Procedure.....	37

3.4. Results and Discussion	43
IV. ENHANCED UNDERSTANDING MIC USING INTERDISCIPLINARY APPROACHES.....	61
4.1. Impact of Organic Acid Production by Fermentative Bacteria on Carbon Steel Corrosion	61
4.2. Integration of Electrochemistry and Microbiology	62
4.3. Enhanced Understanding and Targeted Mitigation	63
4.4. Roles of Thiol and Thiosulfate Metabolism in Corrosion	64
4.5. Integration of Electrochemistry and Microbiology (2).....	64
4.6. Enhanced Understanding and Targeted Mitigation (2)	65
4.7. Future Work.....	66
4.8. Supplemental Information	70
4.9. Conclusions.....	73
REFERENCES	75
APPENDIX	105

LIST OF FIGURES

Figure	Page
1-1: Schematic of SC-ZRA electron transfer	8
2-1: Growth, glucose concentrations, and pH of FE1 after 10 transfers	31
2-2: Current and potential (A, D, G, and J), glucose and acetate concentrations (B, E, H, and K), and pH (C, F, I, and L) in SC-ZRA incubations with bicarbonate buffering that were uninoculated (A-C) or inoculated with FE1 (D-F) and without bicarbonate buffering that were uninoculated (G-I) or inoculated with FE1 (J-L). Current and potential are in red and blue, respectively in panels A, D, G, and J. Glucose and acetate concentrations are depicted by circles and squares, respectively in panels B, D, H, and K. Glucose, acetate, or pH of WE1 chamber and WE2 chamber are depicted by open and closed shapes, respectively, in panels B, C, E, F, H, I, K, and L.	32
3-1: Current (A), potential (B), and pH (C) in SC-ZRA incubations that included the cysteine-metabolizing enrichment culture in synthetic brine with both acetate and cysteine amendment (blue), with cysteine amendment only (red), with acetate amendment only (orange), and with neither acetate nor cysteine (yellow). Closed shapes in panels C represent pH concentrations in the WE1 chamber and open shapes represent pH in the WE2 chamber. Current and potential in uninoculated SC-ZRA incubations are shown in black and are from Chinthala et al. (2024). ...	53
3-2: Scanning electron micrographs and corresponding EDS spectra (below respective micrographs) of WEs recovered from SC-ZRA incubations with the thiol-metabolizing enrichment culture. Panels A and B are WE1 and WE2, respectively, from an incubation with acetate and cysteine, and panels C and D are WE1 and WE2, respectively, from an incubation with acetate only. The x axis of EDS spectra indicates Energy (keV) and the y axis indicates counts. Scale bars in micrographs in panels A, B, C, and D represent 5 μm , 10 μm , 5 μm , and 5 μm , respectively.	55
3-3: Scanning electron micrographs and corresponding EDS spectra (below respective micrographs) of WEs recovered from SC-ZRA incubations with the thiol-metabolizing enrichment culture. Panels A and B are WE1 and WE2, respectively, from an incubation with cysteine, and panels C and D are WE1 and WE2, respectively, from an incubation with no cysteine. The x axis of EDS	

spectra indicates Energy (keV) and the y axis indicates counts. Scale bars in micrographs in panels A, B, C, and D represent 5 μm , 10 μm , 5 μm , and 5 μm , respectively.....56

- 3-4: Current (A), potential (B), and thiosulfate concentration (C) in SC-ZRA incubations that included the thiosulfate reducing enrichment culture with (blue) and without (red) lactate amendment. Closed shapes in panels C represent thiosulfate concentrations in the WE1 chamber and open shapes represent concentrations in the WE2 chamber. Error bars represent one standard error of duplicate measurements. Current and potential in uninoculated SC-ZRA incubations are shown in black and are from Chinthala et al. (2024).....57
- 3-5: Growth (A), thiosulfate (open shapes in B), sulfide (closed shapes in B), and lactate concentrations (C) in uninoculated medium (black), enrichment culture with lactate (blue), and enrichment culture without lactate (red). Error bars represent one standard deviation of triplicate incubations.....58
- 3-6: Infinite focus microscopy (IFM) images of the thiosulfate ZRA carbon steel coupons recovered from SC-ZRA incubations with the thiosulfate reducing enrichment culture with lactate (WE1 panel A and WE2 panel B) and without lactate (WE1 panel C and WE2 panel D) Thiosulfate without lactate: WE2. **
Note of scaling = 1 mm.....59

LIST OF TABLES

Table	Page
1-1: Enzymes involved in fermentative reactions detected in MAGs attributed to <i>C. oceanisediminis</i> , <i>S. epidermidis</i> and <i>L. amygdalina</i>	30
1-2: Treatments and corrosion rate ratios of WE1 and WE2 coupons from SC-ZRA incubations with FE1.	31
2-1: Mass loss and predicted mass loss of electrodes in SC-ZRA incubations.....	54
2-2: Genes detected in MAGs recovered from cysteine metabolizing and thiosulfate reducing enrichment cultures	60

CHAPTER I

BACKGROUND

1.1. The Problem with Corrosion

Corrosion threatens pipelines transporting oil and natural gas, primarily due to their construction using carbon steel (Khan et al., 2021; Kiani Khouzani et al., 2019; Little et al., 2020). Corrosion poses various risks, including structural deterioration, safety concerns, and operational interruptions. Over time, it diminishes the integrity of carbon steel pipelines, culminating in leaks and ruptures that jeopardize workers, surrounding communities, and the environment. The repercussions extend to soil, water, and air contamination, thereby disrupting ecosystems and endangering wildlife (Dennis & Garrelfs, 2014). Corrosion-related maintenance and repair work can also disrupt operations, resulting in downtime and increased costs (Dennis & Garrelfs, 2014; Lahme et al., 2020). Managing corrosion requires proactive measures, advanced technologies, and industry collaboration to ensure pipeline safety, environmental protection, and reliable material transportation (Kip & van Veen, 2015).

1.2. Microbially Influenced Corrosion

Corrosion is an electrochemical process that deteriorates metals through reactions between those metals and aqueous solutions. It requires a cathode, an anode, and an

electrolytic solution for electron and ion movement (P. Zhang et al., 2015). Oxidation (anodic) and reduction (cathodic) reactions occur at the metal surface or nearby (Miller et al., 2018). Electrons transfer between these reactions, with the anodic reaction causing metal oxidation and dissolution, while the cathodic reaction involves electron acceptor reduction (Kiani Khouzani et al., 2019).

Microbially influenced corrosion (MIC) is a process where microorganisms accelerate the corrosion of metals through their metabolic activities. It typically starts with the colonization of metal surfaces by microorganisms that form a biofilm on the metal, creating a conducive environment for corrosion (Flemming, 1996; Little & Lee, 2015). Heterogeneous metal coverage induces the development of localized anodes and cathodes on metal surfaces, driven by the metabolic activities of microorganisms (Duncan et al., 2009; Plugge et al., 2011). Anodic regions are where metal atoms lose electrons and dissolve into the environment (Little & Lee, 2015). For example, Reaction 1 depicts how iron (Fe) is oxidized to ferrous ion (Fe^{2+}).



The electrons travel through the metal to cathodic regions, where they are consumed in reduction (cathodic) reactions (Guan et al., 2016). In some cases of MIC, microbial activities support these cathodic reactions. Sulfate-reducing bacteria (SRB) are an example of corrosion-inducing microorganisms, as they thrive in anaerobic conditions and create cathodic sites by reducing sulfate (SO_4^{2-}) to hydrogen sulfide (H_2S) (Chinthala et al., 2023). Reaction 2 denotes SRB-mediated sulfate reduction to hydrogen sulfide (Chinthala et al., 2023; Little et al., 2020).

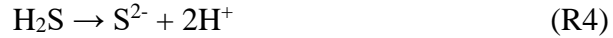


The produced H_2S reacts with ferrous ions at the anode to form iron sulfide (FeS), which precipitates and causes localized corrosion. Reaction 3 denotes the described reaction.

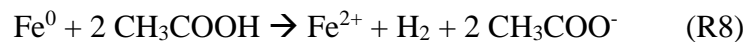


Central to MIC is the interplay between microbial metabolism and electrochemical reactions, where microbial activity disrupts distributions of charges and chemical species in a system where electrochemical reactions occur without any external influence (Boettcher et al., 2021). Microorganisms create and maintain localized anodes and cathodes, enhancing the transfer of electrons, thus intensifying the corrosion process (Dennis & Garrelfs, 2014). This can result in metallic degradation, affecting a wide range of industries and infrastructures. MIC is influenced by various factors that affect its occurrence and severity (Little et al., 2020; Dennis & Garrelfs, 2014).

Some microorganisms may produce corrosive substances which further accelerate corrosion rates (Montville et al., 1985; Madirisha et al., 2022). A proton donor such as hydrogen sulfide (H_2S), or an organic acid releases protons. These protons are then reduced by metallic iron (Fe^0), leading to the degradation of the metal. The process does not depend on the specific type of proton donor but rather on the ability of the metal to reduce the available protons, which drives the corrosion reaction. In this scenario, protons dissociate from hydrogen sulfide (Reaction 4). These protons can then be reduced by iron (R1) to produce hydrogen gas (R5). This process contributes to the corrosion of the iron.



Similar types of microbiological activity can be seen by fermentative bacteria. These bacteria can produce organic acids, like acetic acid (CH_3COOH), which lowers the pH of the environment, increasing the availability of hydrogen ions (H^+). These hydrogen ions participate in the cathodic reaction, accepting the electrons (Suflita et al., 2008). Reaction 5 depicts the reaction of the hydrogen ions accepting the electrons. The production of organic acids enhances the cathodic reduction of hydrogen ions and enhances Fe^{2+} solubility (Suflita et al., 2008; Plugge et al., 2011). Reaction 8 illustrates how protons from acetic acid are reduced, which contributes to iron corrosion, with iron losing electrons and acetic acid gaining them, leading to metal degradation (Suflita et al., 2008).



While proton reduction involves electron transfer and affects the electrochemical balance on the metal surface, the direct attack by organic acids involves chemical dissolution, resulting in the removal of metal ions and the formation of localized acidic environments under biofilms, leading to more aggressive and localized corrosion (Suflita et al., 2008; Plugge et al., 2011). This combined effect of acidic conditions and microbial activity intensifies both metal dissolution and cathodic hydrogen precipitation, thereby

accelerating the overall corrosion rate (Philips, 2020). Environmental conditions, including temperature, pH, salinity, and oxygen levels, also influence MIC by affecting microbial growth and activity (Little & Lee, 2015). Additionally, the properties of the metal substrate, such as composition, surface characteristics, and electrochemical properties, can impact susceptibility to MIC (Lahme et al., 2020). Nutrient and resource availability plays a critical role in determining the presence and type of MIC, specifically influencing whether chemical microbially induced corrosion (CMIC) or electrical microbially induced corrosion (EMIC) occurs (Kip & van Veen, 2015; Xu et al., 2023). For CMIC, Hydrogen (H_2) can be oxidized by certain bacteria (i.e. SRB), which use H_2 as an electron donor in their metabolic processes. In environments where these bacteria are active, they can enhance the cathodic reaction by consuming H_2 at the metal surface. This consumption shifts the equilibrium, promoting further H_2 generation via the cathodic reaction (Reaction 7). As bacteria oxidize H_2 , they maintain a higher rate of electron flow, thereby accelerating the overall corrosion process. In contrast, bacteria EMIC facilitate corrosion by acting as electrical conductors (Xu, 2013). Through the formation of conductive biofilms or nanowires, bacteria can directly transfer electrons from the metal to an electron acceptor, bypassing the need for hydrogen intermediates. This mechanism alters the corrosion dynamics, potentially leading to more rapid metal degradation under certain conditions (Xu, 2013). Whether through H_2 oxidation or direct electron transfer as described by EMIC, bacterial activities ultimately enhance the removal of electrons from the metal, driving the corrosion process. Both pathways

underscore the significant role that microbial activity plays in influencing and accelerating electrochemical reactions at the metal surface.

1.3. Detecting MIC

Electrochemical techniques are powerful tools for detecting and monitoring MIC due to their sensitivity, real-time monitoring capabilities, and ability to assess corrosion processes at the metal-electrolyte interface (Miller et al., 2016). For this research, we used an electrochemical technique known as zero-resistance ammetry (ZRA). ZRA is a technique used for real-time monitoring of corrosion without introducing any resistance into the measurement circuit. This is achieved using highly conductive materials and optimized circuit design, ensuring that the resistance between the working electrodes is negligible. This allows the current to flow freely between the electrodes without any significant voltage drop due to resistance (Chinthala et al., 2023). By minimizing the resistance, ZRA allows for accurate measurement of the current between electrodes. (Chinthala et al., 2023; Miller et al., 2020, 2023)

In a typical ZRA setup, there are two working electrodes (referred to as WE1 and WE2) and a reference electrode (RE), allowing for direct measurement of corrosion current between electrodes when anodic and cathodic conditions develop in the chambers (Miller et al., 2020, 2023). By continuously monitoring corrosion currents, ZRA can detect corrosion associated with microbial activity, providing early warning signs of MIC-induced corrosion (Miller et al., 2020, 2023). Additionally, this technology can distinguish between biotic and abiotic corrosive activities occurring within systems

(Chinthala et al., 2023). ZRA distinguishes between biotic and abiotic corrosion by monitoring electrochemical currents. Biotic corrosion shows currents coincident with microbial activities, while abiotic corrosion produces stable, predictable currents from purely chemical processes. Additionally, ZRA currents observed in abiotic control experiments can be contrasted with those observed with microbial activities.

Metabolites from microbial activity create unique electrochemical reactions detectable by ZRA. By analyzing the current patterns between microbiologically induced anodes and cathodes, ZRA can help identify whether the corrosion is primarily driven by microbial activity or by non-biological factors (Pal & Lavanya, 2022). ZRA helps differentiate the contributions of abiotic and MIC mechanisms by monitoring distinct electrochemical current patterns. When both processes are occurring, ZRA can detect fluctuating currents typically associated with microbial activity alongside the stable, predictable currents of abiotic corrosion, which can be established using abiotic controls. The fluctuating signals arise from microbial metabolites, which create unique electrochemical reactions, while abiotic corrosion produces steady currents due to chemical oxidation or reduction. By analyzing these patterns, ZRA can pinpoint areas where MIC accelerates the anodic or cathodic reactions and assess the overall contribution of microbial activity compared to purely chemical processes. This dual detection capability allows for a more accurate understanding of the dominant corrosion mechanisms in complex environments(Chinthala et al., 2023).

Our ZRA are configured into a split-chamber setup (SC-ZRA). In SC-ZRA, two shorted carbon steel electrodes are placed in separate chambers connected by a

semipermeable membrane or salt bridge. One chamber can be experimentally manipulated (e.g. inoculated with microorganisms), and current is measured between the electrodes (Chinthala et al., 2023). This setup mimics heterogeneous metal coverage by microorganisms, potentially leading to corrosion. The current magnitude reflects the extent of corrosion, while its direction indicates the location of anodic and cathodic processes contributing to corrosion (Miller et al., 2023) Figure 1.1 illustrates electron transfer and current interpretation in a ZRA setup. WE1, containing the bacteria and reference electrode (RE), is the site of bacterial inoculation. A positive current indicates electron transfer from WE1 to WE2, with WE1 as the anode and WE2 as the cathode. A negative current indicates electron transfer from WE2 to WE1, with WE2 as the anode and WE1 as the cathode. For this dissertation work, we used this SC-ZRA setup to understand the corrosive activities of a variety of metabolic types of microorganisms from a natural gas transmission line.

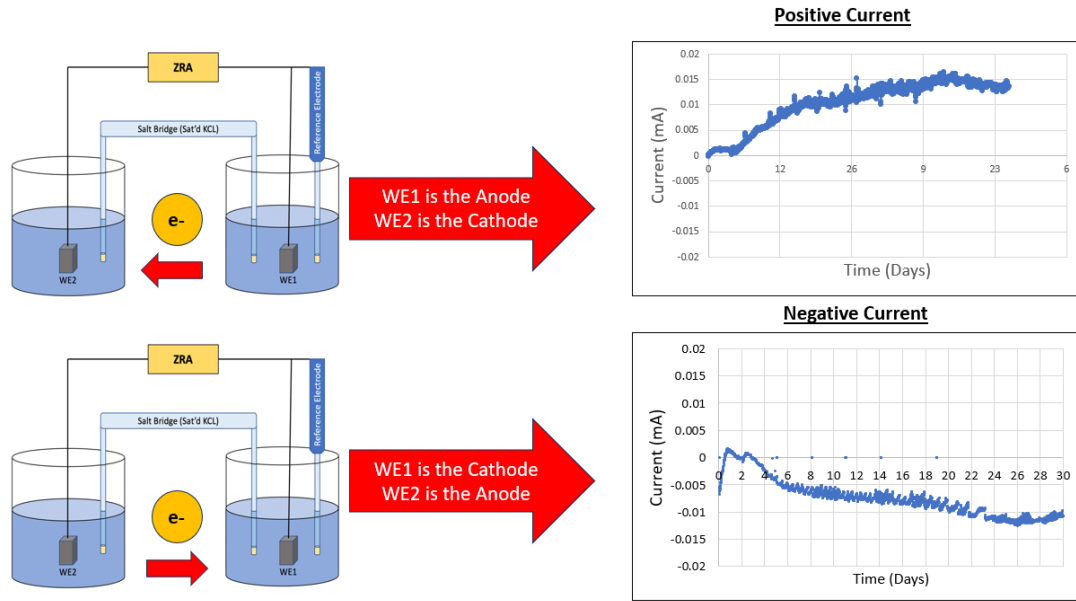


Figure 1-1: Schematic diagram showing electron transfer between working electrodes (WEs) or two ZRA chambers and the resulting current. By convention, WE1 is always the site of bacterial inoculation, as well as where the reference electrode (RE) is located. If current is positive, electron transfer is from WE1 to WE2, indicating that WE1 is the site of the anodic reaction, where metal dissolution is occurring, and WE2 is the site of the cathodic reaction. If current is negative, electron transfer is from WE2 to WE1, with WE2 acting as the anode and WE1 as the cathode. Positive current in the detection of MIC suggests that microbial activity at WE1 is driving anodic corrosion, where the oxidation of metal is being facilitated. If negative current is detected, it suggests that WE1 is experiencing cathodic reactions, meaning that microbial activity is driving reduction processes at the metal surface rather than oxidation. In this case, the metal at WE1 is likely gaining electrons, facilitating reduction reactions such as proton reduction to hydrogen gas (H_2) or the reduction of other oxidizing agents (Chinthala et al., 2023).

1.4. Dissertation Overview

Natural gas transmission lines are crucial infrastructure for transporting gas over long distances, as well as ensuring a reliable supply to residential, commercial, and industrial users (Little & Lee, 2015). However, these pipelines are susceptible to corrosion, which can lead to leaks, ruptures, and potentially catastrophic failures (Xu et al., 2023). Monitoring corrosion in gas transmission lines is challenging due to their extensive length, buried placement, and varying environmental conditions. We seek to understand corrosion mechanisms and develop MIC detection and monitoring tools using SC-ZRA. By utilizing SC-ZRA, we aim to identify and monitor specific corrosion processes in real-time and distinguish between biotic and abiotic processes (Chinthala et al., 2023). Real-time monitoring could allow for more precise and timely interventions, ultimately improving the integrity and safety of gas transmission networks and reducing the risk of environmental damage and economic loss (Enning and Garelfs, 2014; Vigneron, 2016). Here, we enriched for microorganisms of various metabolisms from a natural gas pipeline and determined electrochemical “signatures” of their activities in laboratory SC-ZRA incubations. Ultimately, these signatures will be used to identify MIC in field settings.

Chapter II investigated the impacts of fermentative bacteria from a natural gas pigging pipeline on carbon steel corrosion. Organic acid fermentation products caused corrosion by lowering the pH of the environment. Protons accepted electrons from the metal and form hydrogen gas, which led to corrosion (Suflita et al., 2008). The study monitored glucose depletion, pH decrease, and acetate accumulation during bacterial

fermentation. Observations revealed that organic acid production decreased pH, causing the WE1 electrode to act as a cathode, leading to greater corrosion of WE2 in the SC-ZRA setup. Introducing a sodium bicarbonate buffer neutralized acidity, reducing current generation and corrosion. This research illustrated how fermentative bacteria contribute to corrosion, via the cathodic reduction of hydrogen that is produced during fermentation.

Chapter III examined how S-metabolizing bacteria induced corrosion using SC-ZRA. In oil and gas pipelines, thiosulfate and thiol compounds are commonly present (in addition to sulfate), impacting corrosion when they are metabolized by microorganisms (Laitinen, 1999; Li et al., 2024; Walsh & Giedroc, 2020). Our research aimed to understand the mechanisms of corrosion that occur when these compounds are metabolized. We cultivated two bacterial enrichments from pigging pipeline sludge isolated from a natural gas pipeline. We used ZRA to determine how thiosulfate and thiol metabolism contribute to corrosion.

Thiols, or mercaptans, may undergo degradation, producing free sulfide as a byproduct which can cause corrosion (Tang, 2020; Rucker et al., 2018). A thiol-metabolizing enrichment culture (predominantly *Desulfovibrio alaskensis*) was obtained from a natural gas transmission line and incubated in SC-ZRA experiments in the presence or absence of acetate (as a carbon source) or cysteine (as a model thiol compound). All incubations generated positive current, with the highest current observed in the presence of cysteine (with or without acetate) and was consistent with current observed in abiotic SC-ZRA incubations with sulfide. Acetate in the presence of cysteine

enhanced current and corrosion, likely because it was used as an additional carbon source.

Our study on corrosion under thiosulfate-reducing conditions using SC-ZRA aimed to distinguish between MIC driven by biogenic sulfide and direct electron uptake for thiosulfate reduction. Experiments were conducted with and without lactate (using our enrichment culture containing *Desulfomicrobium* and *Dethiosulfovibrio*) to assess the role of organic carbon. With lactate, thiosulfate reduction was enhanced, potential rose, and negative current indicated electron transfer from WE2 to WE1. Mass loss data confirmed anodic reactions on WE2 and cathodic on WE1, consistent with MIC driven by biogenic sulfide or direct Fe⁰ oxidation coupled to thiosulfate reduction. Without lactate, slight positive current and reduced potential were observed, yet thiosulfate depletion still occurred, suggesting Fe⁰ oxidation coupled to thiosulfate reduction. Thiosulfate may cause abiotic corrosion, so the patterns of current and mass loss indicated competing reactions were occurring on WE1 and WE2.

We analyzed metagenomes from the S-metabolizing enrichment cultures to understand the metabolic potentials of their microbial components. In both cultures, we observed genes encoding enzymes involved in sulfate-reduction, thiosulfate-reduction, thiol degradation, and hydrogenases. While genes encoding extracellular appendages were detected and could support EMIC, we were unable to detect the cytochromes that allow conductivity. Therefore, we hypothesize that Fe⁰ oxidation occurs via H₂ consumption. These results also indicate the metabolic versatility of microorganisms in natural gas transmission lines and indicate that corrosion may occur via reactions of

metal with metabolic products (i.e. cysteine degradation or sulfidogenesis) and use of carbon steel as an electron donor.

Chapter IV discusses the integration of my research among various disciplines using microbiology and electrochemistry to uncover new insights on MIC. By integrating these disciplines, we can understand how microbial processes and electrochemical reactions control MIC. Electrochemistry enables the real time monitoring of MIC (Gajda et al., 2018). By interfacing electrodes with microbial systems, electrochemical techniques can detect and quantify electron transfer events associated with microbial metabolisms (Baranwal & Rajaraman, 2019; Deng et al., 2015). Each chapter of this dissertation focuses on characterizing a microbial metabolism and the electrochemical processes that result from that metabolism, as well as the resulting MIC-related damage that is sustained on the electrode. This interdisciplinary approach allows for the identification of microbial metabolisms involved in corrosion, their products, and how these products influence anodic and cathodic reactions. We anticipate that ZRA measurements can be used to predict MIC before catastrophic failures, and identification of signatures of corrosive microbial activities can facilitate that. Ultimately, this integration improves our ability to protect critical infrastructure from MIC-related damage.

Published manuscripts:

Chinthala, S. P., Sadek, A., Davis, J., Senko, J. M., & Monty, C. N. (2023). Real-time electrochemical monitoring of the progress of sulfate reducing bacterially-induced corrosion of carbon steel. *Corrosion*, 4415. <https://doi.org/10.5006/4415>

Feng, J., Khakipoor, B., May, J., Mulford, M., Davis, J., Siman, K., Russell, G., Smith, A. W., & King, H. (2021). An open-source dual-beam spectrophotometer for

citizen-science-based water quality monitoring. *HardwareX*, 10, e00241.
<https://doi.org/https://doi.org/10.1016/j.ohx.2021.e00241>

Submitted manuscripts:

Davis, J., Chinthala, S. P., Sadek., Senko, J. M., & Monty, C. N. (2024) Electrochemical detection of carbon steel corrosion induced by fermentative bacteria from natural gas transmission lines. *Environmental Microbiology Reports*, submitted.

Manuscripts in preparation:

Davis, J., Chinthala, S. P., Sadek., Senko, J. M., & Monty, C. N. (2024). Electrochemical detection of carbon steel corrosion induced by sulfur-metabolizing bacteria from natural gas transmission lines. *International Biodeterioration and Biodegradation*, in preparation.

Chinthala, S. P., Davis, J., Senko, J. M., & Monty, C. N. (2024). Use of Split Cell Zero Resistance Ammetry to evaluate bio-corrosivity risk in real-world samples. *Corrosion*, in preparation

CHAPTER II

ELECTROCHEMICAL DETECTION OF CARBON STEEL CORROSION INDUCED BY FERMENTATIVE BACTERIA FROM NATURAL GAS TRANSMISSION LINES

2.1. ABSTRACT

The metabolic potential and corrosive activities of a fermentative bacterial enrichment culture from a natural gas transmission line were characterized. Three metagenome assembled genomes (MAGs) attributable to *Cytobacillus*, *Lacrimispora*, and *Staphylococcus* spp. were obtained. These MAGs hosted genes involved in fermentation of carbohydrates to organic acids, and this was reflected in acidification of growth medium by the culture. To evaluate the corrosive activities of the culture, we incubated it in a split chamber-zero resistance ammetry (SC-ZRA) format, which entails the deployment of carbon steel coupons immersed in liquid medium in opposing chambers of an electrochemical cell. Measurement of current between the coupons can then be used to indicate the extent and mechanism of corrosion. When the enrichment culture was added to one side of a SC-ZRA incubation with bicarbonate-buffered medium, pH change and corrosion were minimal. When SC-ZRA incubations were carried out in bicarbonate-free medium, the culture acidified the medium and induced electron transfer from the uninoculated chamber to the inoculated chamber, which was accompanied by mass loss. These results indicate that fermenter-induced MIC is caused by localized fluid

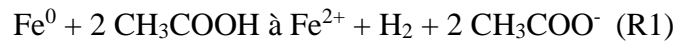
acidification, inducing anodic reactions on the metal surface exposed to the microorganisms and mass loss of the non-exposed metal.

2.2. INTRODUCTION

Microbially influenced corrosion (MIC) of fluid and gas handling equipment and pipelines is a pressing problem in a variety of industrial settings, including food and beverage, wastewater treatment, and oil and gas (Babu et al., 2006; Di Franco et al., 2021; Khan et al., 2021; Kokilaramani et al., 2021). In the oil and gas industry, MIC is often appropriately attributed to the activities of sulfate reducing bacteria (SRB) (e.g., Enning and Garelfs, 2014; Vigneron, 2016, 2018; Little et al., 2020). However, oil and gas processing and transport facilities host metabolically diverse microbial communities (e.g. Duncan et al., 2009; Gieg et al., 2014; Vigneron et al., 2016, 2018). In most settings, the microbial communities that carry out corrosion are complex assemblages of organisms, and in many cases, these involve cooperative interactions between fermentative and sulfate reducing bacteria (Davidova et al., 2012; Vigneron, 2016, 2018). Fermentative bacteria that are encountered in oil and gas handling systems may enhance corrosion by degrading relatively complex organic substrates to H₂ and/or organic acids, thus facilitating the activities of corrosive SRB (Babu et al., 2006; Neria-González et al., 2006; Duncan et al., 2009; Gieg et al., 2014; Lyles et al., 2014; Vigneron et al., 2016, 2018).

Alternatively, fermentative organisms (sometimes referred to as acid producing bacteria) in these communities may contribute to the overall process of MIC via production of

acidic byproducts (Duncan et al., 2009; Gieg et al., 2014; Gu, 2014; Vigneron et al., 2016, 2018; Gu, 2014; Xu et al., 2016; Di Franco et al., 2021). It has been proposed (Gu, 2014; Xu et al., 2016) that a major mechanism of MIC caused by fermentative bacteria occurs under anoxic conditions when organic acid fermentation products (e.g. formic, acetic, lactic acids, etc.) accumulate under low-sulfate conditions. Here, organic acids (depicted as acetic acid for simplicity; Suflita et al., 2008) are reduced by Fe⁰ (R1-R3).



While it is not clear if the protonated acid serves as the electron donor for Fe⁰ oxidation (R1) or if dissociated protons (R2) are the oxidants of Fe⁰ (R3), the ultimate outcome is oxidation of Fe⁰ with H₂ production.

To test the hypothesis that fermentative acid production enhances corrosion, we enriched for fermentative microorganisms from a natural gas transmission line and examined the composition and metabolic potential of the enriched organisms. We then used a split-chamber zero resistance ammetry (SC-ZRA) technique to characterize the corrosive activities of the enrichment culture under chemical conditions approximating those of a gas transmission line. In SC-ZRA, two shorted carbon steel electrodes are deployed in separate, liquid-containing chambers that are connected by a semipermeable membrane or salt bridge (Miller et al., 2016, 2018, 2020). One chamber can be inoculated, and current is measured between the electrodes. In this configuration, SC-ZRA mimics heterogeneous metal coverage by microorganisms, which can lead to

corrosion (Miller et al., 2020, 2023). The magnitude of the current can be indicative of the extent of corrosion, while the direction of current can indicate where anodic and cathodic processes leading to corrosion are occurring (i.e., in the inoculated or uninoculated side of the chamber; Miller et al., 2020; 2023).

2.3. EXPERIMENTAL PROCEDURE

Bacterial cultivation

Natural gas transmission line pigging sludge was used as an inoculum for a fermentative enrichment culture using a medium designed to mimic the high dissolved solids content of aqueous solutions associated with oil and gas extraction, processing, and transport (Chinthala et al., 2023). The brine-based enrichment medium contained 20 mM glucose as a carbon and energy source, and 350 mM NaCl, 30 mM NaHCO₃, 25 mM CaCl₂, 15 mM MgCl₂, 2mM KCl, 0.05 mM K₂HPO₄, 0.07 g/L yeast extract, vitamins, and trace metals (Tanner, 2007). The initial enrichment culture was established using a 10% inoculum of pigging sludge in the brine-based medium. The enrichment culture was maintained through ~15 transfers before it was used in corrosion experiments. In preparation for SC-ZRA experiments, the enrichment culture was grown in 1 L of the brine-based medium to stationary phase. Cells were harvested by centrifugation, then washed, and resuspended 3 times with the brine-based medium. The concentrated cell suspension was then added to incubations to achieve an A₆₀₀ of 1.

SC-ZRA incubations

Carbon steel (UNS G10180) working electrodes (exposed surface area 652 mm²) were prepared for SC-ZRA experiments by polishing them with progressively finer SiC papers of 240, 320, 400, and 600 grits as described in ASTM standard E1558-09 (ASTM, 2014). After obtaining an initial mass, the carbon steel coupons were sterilized by placing them in the SC-ZRA apparatus, replacing air with N₂, and placing the SC-ZRA apparatus (with the steel coupons) in an oven at 160 °C for 4 hours. This process sterilizes the metal, while minimizing any alterations to the metal surface, which occurs during other common sterilization approaches (e.g., autoclaving) (Giai et al., 2016). Brine-based medium (450 mL; described above) was added to both the chambers of the split cell in an anaerobic chamber (Coy Laboratory Products, Grass Lake, MI) and sealed. Where appropriate, sodium bicarbonate was omitted from the brine-based medium. The two chambers of the SC-ZRA were connected by a salt bridge filled with saturated potassium chloride solution. The carbon steel working electrodes (referred to as WE1 and WE2) were included in the respective chambers with a saturated calomel electrode (SCE) as reference electrode in the chamber with WE1. After completing the SC-ZRA setup, the headspace of the chambers was replaced with filter-sterilized 80:20 N₂:CO₂ or N₂ for incubations with and without sodium bicarbonate, respectively. Where appropriate, the WE1 chamber was inoculated with the enrichment culture (called FE1), which was prepared as described above. Current and potential were measured using a BioLogic potentiostat/galvanostat (VSP-300; BioLogic Science Instruments, Seyssinet-Pariset, France) every fifteen minutes. In this configuration, a positive current represents electron

transfer from WE1 to WE2 and a negative current represents electron transfer from WE2 to WE1. Samples were periodically obtained from both chambers to measure pH, glucose, and organic acid concentrations (described below). At the conclusion of the incubations, the WEs were removed subjected to mass loss analysis (described below).

Nucleic acid sequencing and analysis

In preparation for nucleotide sequencing, genomic DNA was extracted from samples using the DNeasy PowerLyzer PowerBiofilm Kit (Qiagen, Germantown, MD). For 16S rRNA gene sequencing, PCR amplification of the 16S rRNA V4 region using the primers 515F (5'-GTG CCA GCM GCC GCG GTA A-3') and 806R (5'-GGA CTA CHV GGG TWT CTA AT-3') (Caporaso et al., 2011) was performed using unique barcodes along with Illumina adapter sequences (Integrated DNA Technologies, Coralville, IA). PCR was performed using a Mastercycler Nexus Gradient (Eppendorf, Enfield, CT) with a 3 min 94°C hot start, followed by 30 cycles of: denaturation at 94°C for 45 sec, annealing at 50°C for 60 sec, and then a 72°C extension for 90 sec, followed by a final extension step at 72°C for 10 min. The PCR products were gel purified and quantified using a Qubit dsDNA HS Assay Kit (Life Technologies, Waltham, MA). Samples were sequenced on an Illumina MiSeq with paired end 250 bp reads. Taxonomic assignments were made by processing raw sequences through QIIME 2 2020.2; (Bolyen et al., 2019) using the q2 quality-filter and deblur plugins to quality filter (Bokulich et al., 2013; Amir et al., 2017) and the q2-feature-classifier (Pedregosa et al., 2011; Bokulich et al., 2018) classify sklearn taxonomy classifier against the Greengenes 18_8 99% OTUs

reference sequences to assign taxonomies to the raw sequences (McDonald et al., 2012; Bokulich et al., 2018).

For metagenomic DNA sequencing, libraries were prepared using Illumina DNA Prep, (M) Tagmentation library preparation kit (Illumina, San Diego, CA) (Haendiges et al., 2020) following the manufacturer's instructions. Initial DNA concentrations were evaluated using the Qubit dsDNA HS Assay Kit (Life Technologies, Waltham, MA). The DNA was then cleaned using DNEasy PowerClean Pro Cleanup Kit (Qiagen, Germantown, MD) and the DNA concentration was analyzed again. Libraries were prepared for each sample by using 30 – 50 ng DNA which underwent simultaneous fragmentation and addition of adapter sequences. These adapters were utilized during a limited-cycle PCR, in which unique indices were added to the sample. Following library preparation, libraries were pooled in equimolar ratios of 0.6 nM and sequenced paired end for 300 cycles using the NovaSeq 6000 system (Illumina, San Diego, CA). Raw metagenomic reads were assessed, trimmed, assembled, quality assessed, binned into putative genomes, quality assessed again, and quality-filtered bins were extracted as assemblies, and taxonomies of both assemblies and raw reads were assigned using Kbase 2.6.4 (Arkin et al., 2018). The following applications were used for each step, respectively: FastQC (v0.11.9), Trimmomatic (v0.36) (Bolger et al., 2014), metaSPAdes (v3.15.3) (Nurk et al., 2017; Prjibelski et al., 2020), CheckM (v1.0.18) (Parks et al., 2015), MetaBAT2 Contig Binning (v1.7) (Kang et al., 2015), CheckM (v1.0.18) (Parks et al., 2015), extract bins as assemblies from BinnedContigs (v1.0.2) (Arkin et al., 2018), GTDB-Tk (v1.7.0) (Parks et al., 2018, 2020; Chaumeil et al., 2019). Kaiju was used to

assign taxonomies using protein-level classifications to sequencing reads by comparing read sequences to the NCBI RefSeq database of completely assembled bacterial, archaeal, and viral genomes (Ondov et al., 2011; Menzel et al., 2016). Metagenome and 16S rRNA sequence data is available at NCBI under BioProject PRJNA1058620.

Analytical techniques

Corrosion rates of WEs were determined by weight loss analysis (WLA) using ASTM method G1-03 (ASTM, 2011). Samples were rinsed with deionized water, wire brushed, and then, immersed in Clarke's Reagent (0.26 M SnCl₂ and 0.07 M Sb₂O₃ in 12.1 M HCl) for 30 seconds to remove surface oxides. After the Clarke's Reagent treatment, the coupons were rinsed with DI water, dried, and weighed. These steps were repeated until no mass was lost between wash cycles, indicating that all oxides were removed (ASTM, 2011). The total mass loss was recorded indicating the physical weight that was lost due to corrosivity of the environment. Corrosion rate was calculated using the following equation:

$$CR = \frac{W * K}{D * A * t} \quad (8)$$

where CR represents the corrosion rate in mm/yr, K (8.76×10^4) is a dimensionless constant, W is the mass loss in grams, A is the exposed surface area of the coupon in cm², T is exposure time in hours and D is the density of carbon steel UNS G10180 in g/cm³ (ASTM, 2011). Subsequently, the corrosion rate ratio (CRR) was calculated by dividing the rate of corrosion by WE1 by the rate of corrosion of WE2. Acetate was quantified by high-performance liquid chromatography by using an Agilent 1200 HPLC system

(Agilent Technologies, Inc. Santa Clara, CA) equipped with an Aminex HPX-87H column (300 mm × 7.8 mm; Bio-Rad Laboratories, Inc.; Hercules, CA) with UV (254 nm) detection (SPD- 10A). A mobile phase of 0.008 N H₂SO₄ was used at a flow rate of 0.6 mL/min. pH was measured using Orion 370 PerpHect pH meter (ThermoFisher Scientific, Waltham, MA).

2.4. RESULTS AND DISCUSSION

Bacterial enrichment and culture composition

In previous work, we reported the enrichment and corrosive activities of microorganisms from natural gas line pigging sludge (Chinthala et al., 2024). To enrich for fermentative microorganisms from the same sample, we used it to inoculate medium that was designed to mimic the aqueous chemistry of the pipeline interior (e.g., 350 mM NaCl). Potential terminal electron acceptors (i.e., oxygen and sulfate) were omitted from the medium and glucose was provided as a fermentative substrate. The enrichment culture (referred to as FE1) was maintained for over 25 transfers. Growth (as indicated by optical density) occurred concurrently with glucose depletion and the culture reached a maximum A₆₀₀ of 1 after 5 d (Figure 2-1A and B). Growth and glucose metabolism caused a decrease in pH of the medium (Figure 2-1B), suggesting that organic acids were products of glucose fermentation. A 16S rRNA partial gene-based survey of the enrichment culture after 15 transfers revealed that it was predominantly composed of Bacillota (54%) and Synergistota (42%).

Metagenomic analysis of enrichment culture

To determine the metabolic potentials of the organisms in the FE1 enrichment culture, we analyzed the metagenome that we recovered from it after 25 transfers. Three metagenome assembled genomes (MAGs) were obtained with coverage of 98%, 100% and 99%, with the largest contig length being 13,261,126 nucleotides. To assess the genomes for completeness and contamination, we used the CheckM application. CheckM can generate clade specific marker genes sets for each bin and reports the taxonomic resolution possible for each bin, which is known as a marker lineage (Parks et al., 2015). CheckM indicated that two of our MAGs had contamination percentages of 1.58% (MAG 1), 1.99% (MAG 2), and 0% (MAG 3). It should be noted that indication of contamination in CheckM are underestimates, and could be responsible for less specificity in the marker lineage identification (Parks et al., 2015). Because our genomes have high completeness, the estimated extents of contamination of the MAGs are likely accurate. To taxonomically assign our MAGs, we used the Genome Taxonomy Database Toolkit (GTDB-Tk), which uses the bacterial and archaeal reference trees, multiple sequence alignments, and taxonomy provided through the GTDB (Chaumeil et al., 2019). MAGs were taxonomically assigned to *Cytobacillus oceanisediminis* (MAG 1), *Lacrimispora amygdalina* (MAG 2), and *Staphylococcus epidermidis* (MAG 3), all three of which are affiliated with the Bacillota, which was the predominant phylum in the partial 16S rRNA gene-based survey. These three taxa appear to be the predominant components of the enrichment culture, because most raw sequence reads were assigned to *C. oceanisediminis* (13%), *L. amygdalina* (33%), and *S. epidermidis* (9%), using Kaiju

(Ondov et al., 2011; Menzel et al., 2016), with 30% unassignable at the species level, and the remaining sequences assigned to taxa comprising less than 2% of the sequence reads. Indeed, when we decreased the completeness threshold to 60% and increased the contamination threshold to 40%, only the MAGs attributable to *C. oceanisediminis* (13%), *L. amygdalina* (33%), and *S. epidermidis* (9%) could be obtained. *C. oceanisediminis* is an aerobic, spore-forming, mesophilic bacterium found in marine sediment. (Lee et al., 2012). *Lacrimispora* spp. are cosmopolitan Gram-positive anaerobes that has been isolated from wastewater treatment plants sludge and animal hosts (Palop et al., 1989; Cornick et al., 1994; Parshina et al., 2003), while *S. epidermidis* is a Gram-positive commensal bacterium that has been isolated from soil, water, and various surfaces in non-human settings (Kloos, 1980; Prussin and Marr, 2015; Gerken et al., 2022). The recovery of these taxa from the gas pipeline is reflective of a physicochemical setting that is impacted by human activities with high dissolved solids (Brown et al., 2012; Thapaliya et al., 2017; Martin et al., 2021). We screened MAGs for enzymes involved in carbohydrate metabolism, particularly those yielding organic acid byproducts that could cause carbon steel corrosion (Madirisha et al., 2022). All three MAGs contained complete Emden-Meyerhof-Parnas pathways, and potential pathways of fermentation product formation by each of the three MAGs are shown in Table 1-1. Metabolic characterization of a strain of *C. oceanisediminis* (H2^T) indicated it metabolized a variety of carbohydrates under oxic conditions, but anaerobic fermentation products were not evaluated (Zhang et al., 2010). Genomic characterization *C. oceanisediminis* 2691 revealed phosphotransferase systems for glucose metabolism and

pathways for mixed acid fermentation of glucose to acetate, ethanol, and lactate (Lee et al., 2012). The MAG attributable to *C. oceanisediminis* in our enrichment can produce acetate, lactate, and succinate from glucose fermentation, but pathways for ethanol, formate and butyrate production are absent or incomplete (Table 1-1). *Lacrimispora* (formerly *Clostridium*) spp. have been isolated from sewage sludge and industrial mudpits, and can ferment carbohydrates to ethanol, acetate, lactate, and butanol (Parshina et al., 2003; Jin et al., 2023). The *L. amygdalina*-attributable MAG in our enrichment contained incomplete pathways for fermentation of glucose to succinate and butyrate, but included genes necessary for glucose fermentation to acetate, ethanol, lactate, and formate (Table 1-1). As human commensals, Staphylococci are encountered in human-impacted and built environments (Kloos, 1980; Prussin and Marr, 2015; de Sousa et al., 2017; Gerkin et al., 2022). *S. epidermidis* strains ferment glucose to lactate, but may produce, acetate, formate, and ethanol (Sivakanesan and Dawes, 1980; Pedroza-Dávila et al., 2020). The *S. epidermidis*-attributable MAG harbored complete pathways for fermentation of glucose to acetate, ethanol, lactate, succinate, and formate, but the pathway for butyrate production was incomplete (Table 1-1). These observations indicate acidification of medium during growth of FE1 was attributable to the accumulation of organic acids by the three MAGs recovered from the enrichment, and these activities could influence corrosion in steel pipelines.

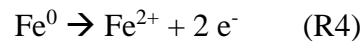
Corrosive activities of FE1 under fermentative conditions

To evaluate the corrosive activities of our culture, we carried out a series of SC-ZRA incubations. In uninoculated SC-ZRA incubations with bicarbonate-containing

synthetic brine, current was initially slightly positive, but no glucose metabolism or pH change were detected (Figure 2-2A-C). Consistent with this lack of activity was the similarity in rates of corrosion of WE1 and WE2 (as indicated by CRR; Table 1-2). When synthetic brine was inoculated with FE1, glucose was metabolized but no decrease in pH was observed in either the WE1 or WE2 chamber (Figure 2-2B and C). Despite the activity of FE1, slight positive current was observed, indicating minimal transfer of electrons from WE1 to WE2. Slightly greater corrosion was observed on WE1 compared to WE2 (as indicated by CRR; Table 1-2), indicating that direct exposure of the WE1 electrode to FE1 minimally enhanced its corrosion rate. Taken together, these results indicate little microbially-induced corrosion (whether determined by corrosion rate or electrochemically) was occurring in the bicarbonate-buffered system.

We hypothesized that the bicarbonate in the synthetic brine was limiting pH change, and therefore corrosion of the carbon steel coupons. To test this hypothesis, we conducted a second series of SC-ZRA incubations without bicarbonate in the brine. In SC-ZRA incubations without bicarbonate buffering, and no FE1 inoculation, the starting pH was lower than incubations with bicarbonate added, and it changed minimally over the course of the incubations (Figure 2-2I). Glucose was not consumed, and no organic acid accumulation was observed (Figure 2-2H). Similarly low current to the uninoculated incubation with bicarbonate was observed, indicating that WE1 and WE2 were in electrochemical equilibrium, which is consistent with the CRR of 0.9 (Table 1-2). When FE1 was added to the WE1 chamber of an SC-ZRA incubation, glucose metabolism proceeded in the WE1 chamber, accompanied by accumulation of acetic acid (Figure 2-

2K). The accumulation of organic acid resulted in a pH decrease to approximately 4.5 in the WE1 chamber, but not the WE2 chamber (Figure 2-2L). We were unable to detect succinate, butyrate, lactate, or formate as products of glucose metabolism during the SC-ZRA incubations. All three MAGs recovered from the enrichment were capable of fermentation of glucose to acetate, which is consistent with the observation of acetate accumulation. However, low pH (i.e., <5) may modify the fermentation product profiles of *Lacrimispora* spp. (Jin et al., 2023). The pH decrease enhanced the development of negative current, indicating electron transfer from WE2 to WE1 (Figure 2-2J). This pattern of electron transfer is consistent with cathodic reactions R1-R3 occurring in the WE1 chamber, and the anodic reaction (R4) occurring in the WE2 chamber.



Here, the decrease in pH provides a driving force for hydrogen generation and the Fe⁰ corrodes on the WE2 to maintain equilibrium. The CRR of the WEs (Table 1-1) was consistent with this negative current, where WE2 (the anode) was corroding more rapidly than WE1 (the cathode).

Implications for MIC by fermentative microorganisms

Fermentative bacteria are encountered in a variety of oil/gas handling and other industrial settings and are important mediators of organic carbon degradation (Duncan et al., 2009; Gieg et al., 2014; Gu, 2014; Vigneron et al., 2016, 2018; Di Franco et al., 2021). This can include organisms that ferment carbohydrates and other types of non-hydrocarbon organic compounds (Duncan et al., 2009; Gieg et al., 2014; Vigneron et al., 2016, 2018).

While hydrocarbons are generally the predominant organic substrate in oil and gas, a far wider variety of organic compounds may be metabolic substrates, including compounds used in oil and gas extraction, transport, and processing, as well as microbial cross-feeding (Annuk and Moran, 2010; Luek and Gonsior, 2017; Fritts et al., 2021; Li et al., 2023). In any case, organic acids are important products of organic carbon metabolism and may cause corrosion.

The results of this work illustrate the dynamics of MIC under fermentative conditions. First, we have shown that localized acidification induces cathodic reactions (R1-R2), thus inducing mass loss via R4. The SC-ZRA approach allowed us to mimic the conditions of localized fermentative activity on a metal surface, which induces localized corrosion. Second, we show that the activities of fermentative bacteria can cause corrosion independently of their metabolic relationships with SRB. Third, the work illustrates the influence of pH and buffering on fermenter-induced MIC. In oil and gas extraction and processing settings, pH and alkalinity can vary dramatically. In most cases, the pH and alkalinity of brines is influenced by the dynamics of the carbonic acid system, although carboxylic acids can also influence the alkalinity of brines (Sanchez-Rosario and Hildebrand, 2022; Zhang et al., 2019; Maskari et al., 2020; Thyne and Brady, 2016). pH of produced waters typically falls in a range of 4-8, but extremes below 2 and above 8 have been reported (Li, 2013; Alley et al., 2011; Emam et al., 2014). Alkalinities can range from 0-5000 meq/L (Sanchez-Rosario and Hildebrand, 2022; Zhang et al., 2019) and are a reflection of the oil/gas host rock and associated brine. Brines/production waters from carbonate-rich reservoirs will have higher alkalinities

(Maskari et al., 2020; Thyne and Brady, 2016). Post-extraction degassing of CO₂ will also influence pH and alkalinity (de Paula Cosmo et al., 2022). The work we present here illustrates how variability in pH and buffering of brines and production waters could control the extents of corrosion by fermentative microorganisms from gas transmission lines.

Conclusion

This work illustrates the role of fermentative bacterial activities in MIC that is independent of SRB. When production of organic acid metabolites decreases the pH of solutions, corrosion occurs via the development of localized anodes and cathodes on metals. In the case of fermenter-induced MIC, acid production causes the development of anodic conditions in proximity to the bacterial activities.

Table 1-1: Enzymes involved in fermentative reactions detected in MAGs attributed to *C. oceanisediminis*, *S. epidermidis* and *L. amygdalina*.

Metabolism and enzymes	MAG 1 (<i>C.</i> <i>oceanisediminis</i>)	MAG 2 (<i>L.</i> <i>amygdalina</i>)	MAG 3 (<i>S.</i> <i>epidermidis</i>)
Acetate production			
Phosphate acetyl transferase	+	+	+
Acetate kinase	+	+	+
Ethanol production			
Acetaldehyde dehydrogenase	+	+	-
Alcohol dehydrogenase	-	+	+
Lactate production			
Lactate dehydrogenase	+	+	+
D-lactate dehydrogenase	-	-	+
Succinate production			
Malate dehydrogenase (quinone)	+	-	+
Malate dehydrogenase (oxaloacetate-decarboxylating)	+	+	+
Malate dehydrogenase (Oxaloacetate-decarboxylating) (NADP ⁺)	+	-	+
Fumarate hydratase	+	-	+
Formate production			
Formate acetyltransferase (pyruvate-formate lyase)	-	+	+
Pyruvate formate lyase activating enzyme	-	+	+
Butyrate production			
Pyruvate-ferredoxin oxidoreductase	-	+	-
Acetyl-CoA C-acetyltransferase	+	+	+
3-Hydroxybutyryl-CoA dehydrogenase	+	-	-
4-Hydroxybutyryl-CoA dehydratase	-	+	-
Butyryl-CoA dehydrogenase	+	-	-
Phosphotransbutyrylase	+	-	-
Butyrate kinase	+	+	-

Table 1-2. Treatments, corrosion rates, and corrosion rate ratios (CRR) of WE1 and WE2 coupons from SC-ZRA incubations with FE1. Corrosion rates are shown parenthetically below CRR.

Bicarbonate addition	WE1 treatment	WE2 treatment	Corrosion Rate Ratio (WE1:WE2)
With bicarbonate	Uninoculated	Uninoculated	1.0 (35 mpy/35 mpy)
With bicarbonate	Inoculated with FE1	Uninoculated	1.3 (42 mpy/32 mpy)
Without bicarbonate	Uninoculated	Uninoculated	0.9 (38 mpy/42 mpy)
Without bicarbonate	Inoculated with FE1	Uninoculated	0.5 (13 mpy/26 mpy)

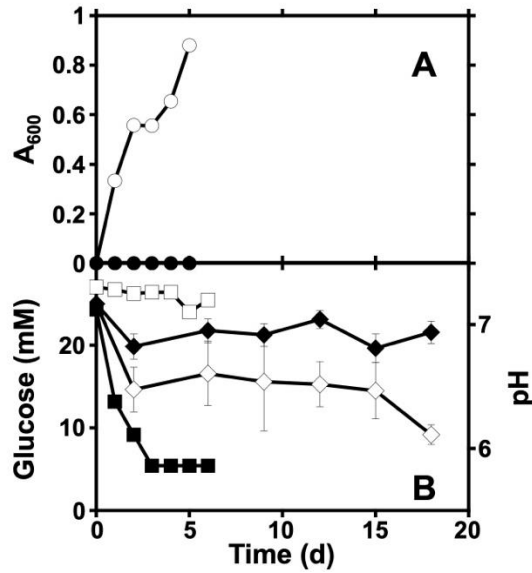


Fig. 2-1. Growth (as indicated by A_{600} ; circles in panel A), glucose concentrations, and pH (diamonds and squares, respectively in panel B) of FE1 after 10 transfers. Filled and open shapes represent values in uninoculated and inoculated media, respectively. Error bars represent standard deviations of duplicate measurements.

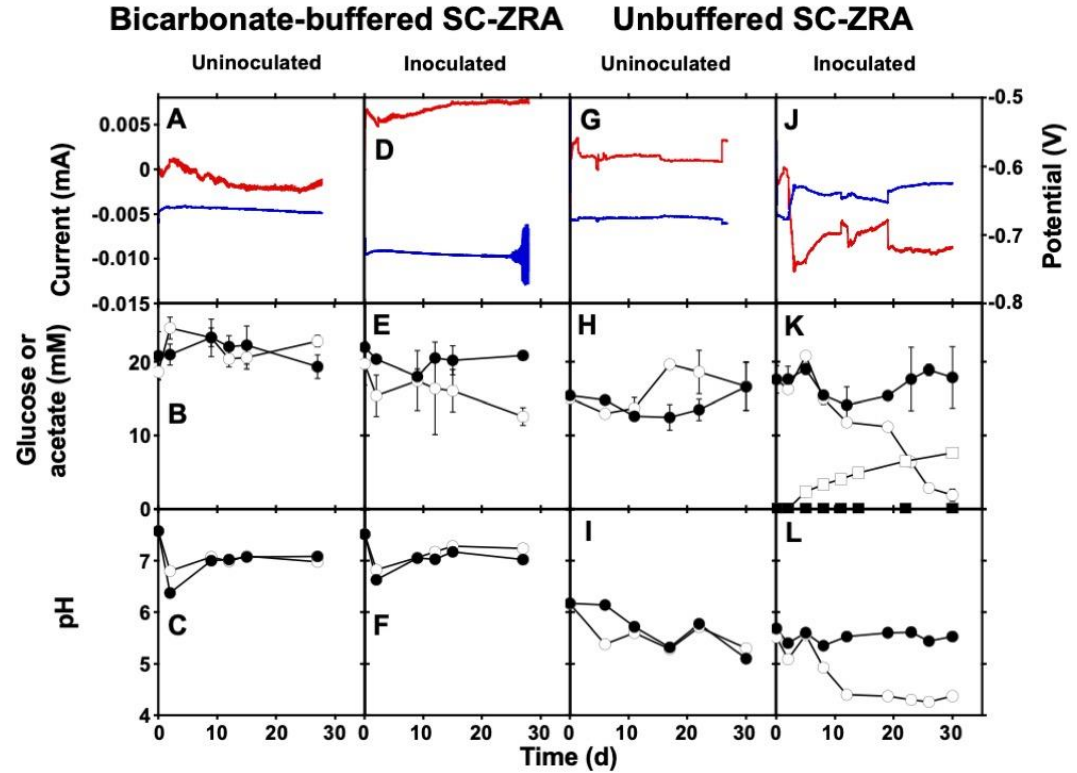


Fig. 2-2. Current and potential (A, D, G, and J), glucose and acetate concentrations (B, E, H, and K), and pH (C, F, I, and L) in SC-ZRA incubations with bicarbonate buffering that were uninoculated (A-C) or inoculated with FE1 (D-F) and without bicarbonate buffering that were uninoculated (G-I) or inoculated with FE1 (J-L). Current and potential are in red and blue, respectively in panels A, D, G, and J. pH and glucose concentrations are depicted by open (WE1 chamber) and closed (WE2 chamber) circles in their respective panels. Acetate concentrations are depicted in panel K using open (WE1 chamber) and closed (WE2 chamber) squares.

CHAPTER III

PATHWAYS OF CORROSION INDUCED BY THIOSULFATE REDUCING AND THIOL METABOLIZING BACTERIA

3.1. ABSTRACT

Thiol compounds and thiosulfate are routinely encountered in oil and gas transmission lines and may support microbially influenced corrosion (MIC), but corrosion caused by these organisms is not as extensively studied as that caused by sulfate reducing bacteria. The corrosive activities of thiol and thiosulfate metabolizing bacterial enrichment cultures derived from natural gas pipeline pigging sludge were assessed. Through 16S rRNA gene surveys and metagenomic analyses, the thiol-metabolizing culture was enriched on cysteine as a substrate and found to be dominated by *Desulfovibrio alaskensis*. Metagenomic characterization of the enrichment culture indicated that it could metabolize cysteine to ammonium, pyruvate, and free sulfide. The latter induced corrosion in split chamber-zero resistance ammetry (SC-ZRA) incubations, which use the current arising from microbiological activities to indicate corrosion. The thiosulfate-reducing culture was enriched with lactate as an electron donor and primarily composed of *D. ferrophilus*, which SC-ZRA incubations indicated oxidized Fe⁰ coupled with thiosulfate reduction. Analysis of the metagenome of the enrichment culture indicated abundant hydrogenase-encoding genes, suggesting that cathodically produced H₂ was

servicing as an intermediate in Fe^0 oxidation. Additionally, thiosulfate itself was corrosive, giving rise to patterns of current that were distinct from those observed during Fe^0 oxidation under sulfate reducing conditions. These findings demonstrate that thiol and thiosulfate metabolism contribute to microbially-induced corrosion (MIC) through distinct mechanisms, with implications for understanding corrosion processes in oil and gas systems.

3.2. INTRODUCTION

Microbiologically induced corrosion (MIC) is a major cause of the deterioration of steel used for petroleum and natural gas transport, handling, and processing equipment (Videla, 2002). An estimated 20% of all corrosion in aqueous systems is caused by microbiological activities (Flemming, 1996), which may account for billions of US dollars in damage (Dennis & Garrelfs, 2014; Little et al., 2020). In addition to monetary costs, release of toxic substances due to MIC damage to pipelines is an environmental concern (Duncan et al., 2009). Sulfate reducing bacteria (SRB) are widely implicated catalysts of MIC in oil and gas handling and storage systems (Dennis & Garrelfs, 2014). Besides sulfate, oil and gas environments contain other sulfur-containing species, including thiols and thiosulfate, which may also influence corrosion (Duncan et al., 2009; LaButti et al., 2010; Machuca et al., 2017; Tran et al., 2022; Li et al., 2024). Despite their potential significance, the roles of these compounds in MIC remain less understood than the roles of sulfate and sulfate reduction in MIC.

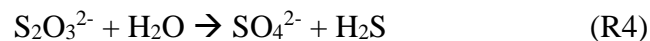
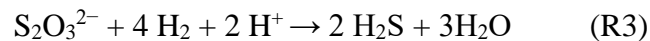
Thiols are organic compounds characterized by a sulfhydryl group (-SH) bound to a carbon atom (Tang, 2020). These compounds are commonly found in oil and gas systems and are structurally and compositionally diverse (Shi and Wu, 2021; Li et al., 2024). A variety of microorganisms can enzymatically remove these thiol groups via a variety of enzymes classified as carbon-sulfur lyases (Klose et al., 2011; Oguri et al., 2012; Bocian-Ostrzycka et al., 2017; Boden and Hutt, 2019; Takagi and Ohtsu, 2017; Biwer et al., 2022), whose activity is depicted in R1 using mercaptopyruvate as a model.



Here, degradation of the thiol compound yields free sulfide as a product (Rücker et al., 2018). Notably, in R5, the S is not dissimilatory metabolized, but the pyruvate can be subsequently metabolized. Nevertheless, a product of this activity is free sulfide, which can induce corrosion by reacting with the Fe^0 of a pipeline, yielding FeS and H_2 (R2).



Thiosulfate may be reduced as a terminal electron acceptor to sulfide (R3 using H_2 as an electron donor, but could be various organic electron donors; Choudhary et al., 2015; Zhang et al., 2020; Laitinen, 1999) or disproportionated to sulfate and sulfide (R4; Jackson and McInerney, 2000).



In both cases, the sulfide product can induce corrosion as depicted in R2. Alternatively, Fe⁰ can be used as an electron donor (directly or indirectly) to support thiosulfate reduction (R4; Enning and Garrelfs, 2014).



When Fe⁰ is used as an electron donor, it may be directly oxidized, a process referred to as electrochemical MIC (EMIC), or via H₂ as a chemical intermediate in Fe⁰ oxidation, referred to as chemical MIC (CMIC; Enning and Garrelfs, 2014). In the case of CMIC microbiological consumption of H₂ (R3) enhances the acid attack of Fe⁰ (e.g. R2).

Mechanisms and extents of MIC can be determined by a split-chamber zero-resistance ammetry (SC-ZRA) approach (Miller et al., 2016, 2018, 2020; Chinthala et al., 2024). With SC-ZRA, two carbon steel electrodes are placed in separate liquid-containing chambers connected by a membrane or salt bridge (Miller et al., 2016, 2018, 2020). The conditions of the chambers can be experimentally manipulated, and the direction and magnitude of the current that arises between the two electrodes can be used to identify anodic or cathodic reactions in the respective chambers and the extent of corrosion (Chinthala et al., 2024). By inoculating one chamber with microorganisms, the SC-ZRA mimics the heterogeneous microbiological coverage of metal surfaces that can lead to localized cathodic and anodic regions of the metal, which leads to localized corrosion (Chinthala et al., 2024, Miller et al., 2016). Previous experiments with the SC-ZRA and SRB showed that cathodic corrosive reactions occurred on the electrode exposed to SRB activities (Chinthala et al., 2024). In this study, we investigated the corrosive potential

and activities of thiol compound metabolizing and thiosulfate reducing bacteria. We developed enrichment cultures targeting these metabolisms from natural gas transmission line pigging sludge and used metagenomic surveys to examine their metabolic potentials. We then used the SC-ZRA technique to assess the corrosive activities of the enrichment cultures.

3.3. EXPERIMENTAL PROCEDURE

Thiosulfate enrichment culture. Pigging sludge from a natural gas transmission line was used to inoculate enrichment cultures. A synthetic brine-based medium was designed to replicate the high salinity of oil and gas extraction-associated fluids (Chinthala et al., 2024). The synthetic brine contained 350 mM NaCl, 30 mM NaHCO₃, 15 mM MgCl₂, 2mM KCl, 0.05 mM, K₂HPO₄, 25 mM CaCl₂, and was used as the basis for enrichment media. The thiol-metabolizing enrichment medium included 20 mM sodium acetate as a carbon source, 8 mM cysteine-HCl as a model thiol compound, 5 mM NH₄Cl and 100 mM sodium 2-[4-(2-hydroxyethyl) piperazin-1-yl] ethane-1-sulfonate (HEPES). The thiosulfate reducing bacterial enrichment medium included 10 mM Na₂S₂O₃ and 20 mM sodium lactate as an electron donor vitamins and trace metals (Tanner, 2007). O₂ was removed from media by bubbling with 80:20 N₂: CO₂, and media were dispensed into serum bottles or tubes, where they were sealed under a headspace of the same gas. Media were sterilized by autoclaving. Enrichments were maintained for 15-20 transfers before use in SC-ZRA experiments (described below). For experiments to determine growth patterns of the enrichment cultures, samples were periodically removed and analyzed as described below. In preparation for SC-ZRA experiments, enrichment

cultures were grown in 1000 mL of their respective brine-based media to stationary phase. Cells were then harvested by centrifugation, and washed and resuspended 3 times with synthetic brine. The concentrated cell suspension was subsequently added to the SC-ZRA incubations (described below) to achieve an A_{600} of 1.

16S rRNA sequencing and metagenomics. Genomic DNA was extracted using the DNeasy PowerLyzer PowerBiofilm Kit (Qiagen, Germantown, MD). 16S rRNA genes were amplified by PCR targeting the 16S rRNA V4 region with primers 515F (5'-GTG CCA GCM GCC GCG GTA A-3') and 806R (5'-GGA CTA CHV GGG TWT CTA AT-3') (Caporaso et al., 2011). PCR utilized unique barcodes and Illumina adapter sequences (Integrated DNA Technologies, Coralville, IA). PCR amplification was carried out using a Mastercycler Nexus Gradient thermocycler (Eppendorf, Enfield, CT) with the following steps: a 94°C hot start for 3 minutes, 30 cycles of denaturing at 94°C for 45 seconds, annealing at 50°C for 60 seconds, extension at 72°C for 90 seconds, and final extension at 72°C for 10 min. Gel-purified PCR products were quantified using a Qubit dsDNA HS Assay Kit (Life Technologies, Waltham, MA), followed by sequencing on an Illumina MiSeq with paired end 250 bp reads. Taxonomic assignments were made using QIIME 2 2020.2 with the q2 quality-filter, deblur plugins, and q2-feature-classifier against Greengenes 18_8 99% OTUs reference sequences (Bolyen et al., 2019).

For metagenomic DNA sequencing, libraries were prepared with the Illumina DNA Prep, (M) Tagmentation library preparation kit (Illumina, San Diego, CA) (Haendiges et al., 2020) following the manufacturer's instructions (Haendiges et al., 2020). DNA concentrations were determined using the Qubit dsDNA HS Assay Kit (Life

Technologies, Waltham, MA). Subsequently, DNA was cleaned with the DNEasy PowerClean Pro Cleanup Kit (Qiagen, Germantown, MD), and its concentration was reanalyzed. Libraries for each sample were created using 30 – 50 ng DNA, which underwent simultaneous fragmentation and adapter sequence addition through a limited-cycle PCR, incorporating unique indices to each sample. After preparation, libraries were pooled in equimolar ratios of 0.6 nM and sequenced paired end for 300 cycles using the NovaSeq 6000 system (Illumina, San Diego, CA).

Raw metagenomic reads obtained above were trimmed, assessed, assembled into contigs, quality-assessed, binned into putative genomes, putative genomes/bin were quality-assessed for completeness (>90%) and contamination (<5%). The bins were extracted as assemblies and taxonomies of both metagenome-assembled genomes (MAGs), and raw reads were assigned using Kbase 2.6.4 (Arkin et al., 2018). The following applications were used for each step, respectively: FastQC (v0.11.9), Trimmomatic (v0.36) (Bolger et al., 2014), metaSPAdes (v3.15.3) (Nurk et al., 2017; Prjibelski et al., 2020), MaxBin2 Contig Binning (v2.2.4) (Wu et al., 2014), CheckM (v1.0.18) (Parks et al., 2015), BinUtil (extract bins as assemblies from BinnedContigs) (v1.0.2) (Arkin et al., 2018). CheckM was used to estimate coverage and extents of contamination, and may underestimate contamination, potentially leading to reduced specificity in marker lineage identification (Parks et al., 2015) but given the high completeness of our genomes (95-100%), it is likely that the reported levels of contamination of the MAGs are accurate. For taxonomic assignment of our MAGs, we used the Genome Taxonomy Database Toolkit GTDB-Tk (v1.7.0) (Parks et al., 2018,

2020; Chaumeil et al., 2019), which cross-references bacterial and archaeal reference trees, along with multiple sequence alignments and taxonomy information derived from the GTDB (Chaumeil et al., 2019). Genes were located based on the metabolic pathway associated with the observed activity of the experiments. For example, if thiosulfate reduction was occurring, all genes pertinent to thiosulfate reduction were identified and verified to see if the pathway was complete. Once the MAGs were annotated via DRAM (v.0.1.2) for Annotating and Distilling Genomes, genes were called by manually searching for the desired gene associated with the pathway. This was by way of the application's creation of an interactive functional summary per genome. Because some genes are referred to by multiple names, multiple searches were performed to verify the presence or absence of a certain gene. Genes were also categorized and sub-categorized by their metabolic pathways and gene function. Metagenome and 16S rRNA sequence data is available at NCBI under BioProject PRJNA1156014.

SC-ZRA experiments. In preparation for SC-ZRA experiments, carbon steel (UNS G10180) working electrodes with an exposed surface area of 652 mm² were polished using SiC papers (240, 320, 400, and 600 grit papers, progressively) following ASTM standard E1558-09 (ASTM, 2014). After initial mass measurements, the carbon steel coupons were sterilized in the SC-ZRA apparatus in an oven at 160°C for 4 hours under N₂. This sterilization process minimizes alterations of the metal surface (Giai et al., 2016).

SC-ZRA assemblies were taken into an anaerobic chamber (Coy Laboratory Products, Grass Lake, MI), synthetic brine (described above) was added to both split cell

chambers (~400 mL), and the assemblies were resealed. For SC-ZRA incubations that included the thiosulfate-reducing enrichment culture, 10 mM Na₂S₂O₃ and 20 mM sodium lactate (where appropriate) were added to the brine. For SC-ZRA incubations that included the thiol-metabolizing enrichment culture, 20 mM sodium acetate and 8 mM cysteine-HCl (where appropriate) were added to the brine. The SC-ZRA chambers were connected by a salt bridge containing a saturated potassium chloride solution. Carbon steel working electrodes (WE1 and WE2) and a saturated calomel electrode (SCE; in the WE1 chamber) were immersed in the synthetic brine. Upon removal from the anaerobic chamber, the headspace of SC-ZRA incubations was replaced with filter-sterilized 80:20 N₂: CO₂. Where appropriate, the WE1 chamber was inoculated with the enrichment culture as described above. Current and potential were measured using a BioLogic potentiostat/galvanostat (VSP-300; BioLogic Science Instruments, Seyssinet-Pariset, France) every fifteen minutes. In this setup, a positive current indicates electron transfer from WE1 to WE2, while a negative current indicates electron transfer from WE2 to WE1. Samples from both chambers were collected periodically to measure pH, thiosulfate concentrations and acetate concentrations (described below). After incubations, the WEs were removed for mass loss analysis and profilometric characterization of the coupon surface as described below.

Analytical techniques. For growth experiments, subsamples of enrichment cultures were periodically collected using a needle and syringe. The optical density at 600 nm (OD₆₀₀) of cultures was measured using an VWR V-3000 spectrophotometer (Avantor, Radnor, PA). pH of suspensions was measured using an Orion 370 PerpHect

pH meter (ThermoFisher Scientific, Waltham, MA). Solids were removed from suspension of samples intended for measurement of lactate, sulfate, sulfite, and thiosulfate by centrifugation. Sulfate, sulfite, and thiosulfate were quantified in the supernatant using a Dionex ICS-1100 ion chromatography system with an IonPac CS12A column and conductivity detection meter (Thermo Fisher, Waltham, MA). Lactate in the supernatant was quantified by high-performance liquid chromatography using an Agilent 1200 HPLC system (Agilent Technologies, Inc. Santa Clara, CA) equipped with an Aminex HPX-87H column (300 mm × 7.8 mm; Bio-Rad Laboratories, Inc.; Hercules, CA) with UV (254 nm) detection (SPD- 10A). A mobile phase of 0.008 N H₂SO₄ was used at a flow rate of 0.6 mL/min. Samples intended for measurement of sulfide were placed in 4% zinc acetate before spectrophotometric measurement of sulfide using the methylene blue assay (Cline, 1969). Samples were collected from SC-ZRA incubations and processed in the same way as described above.

To prepare coupons for surface examination by scanning electron microscopy (SEM), coupons were immersed in anoxic glutaraldehyde solution (2%) for 1 day at 4 °C, dehydrated using a critical point dryer, sputter-coated with platinum. Coupons were visualized using Tescan LYRA-3 XMU FIB-FESEM SEM system (Tescan, Czech Republic). After performing weight loss analysis (described below), coupons are analyzed for pitting features using infinite focus microscopy (IFM) using an Alicona InFocus G5 instrument (Bruker Alicona, Itaska, IL).

Corrosion rates of working electrodes (WEs) were determined using weight loss analysis (WLA) with ASTM method G1-03 (ASTM, 2011). For WLA, each electrode

was rinsed with deionized water, wire brushed to remove tougher surface particulates, and then immersed in Clarke's Reagent (0.26 M SnCl₂ and 0.07 M Sb₂O₃ in 12.1 M HCl) for ~30 seconds to remove surface oxides. Following Clarke's Reagent treatment, the coupons were weighed. These steps were repeated until no mass was lost between wash cycles, indicating the removal of all oxides (ASTM, 2011). Corrosion rate was calculated using the following equation:

$$CR = \frac{W * K}{D * A * t}$$

The corrosion rate (CR) was calculated in mm/yr using the formula $CR = (K \times W) / (A \times T \times D)$, where K (8.76×10^4) is a dimensionless constant, W is the mass loss in grams, A is the exposed surface area of the coupon in cm², T is the exposure time in hours, and D is the density of carbon steel UNS G10180 in g/cm³ (ASTM, 2011).

3.4. RESULTS AND DISCUSSION

Enrichment cultures Using pigging sludge from a natural gas transmission line, we inoculated brine-based media targeting cysteine fermenting or lactate oxidizing thiosulfate reducing bacteria. A 16S rRNA survey of the thiol metabolizing enrichment culture after 15 transfers revealed that it was composed almost entirely (99%) of *Desulfovibrio* (now *Oleidesulfovibrio*) *alaskensis*, which is a well-characterized sulfate reducing bacterium that was originally isolated from a soured oil well in Prudhoe Bay, Alaska (Feio et al., 2004). A MAG attributable to *D. alaskensis* (MAG 1) was also recovered from the culture with 99% completeness and 2% contamination. In addition, four additional MAGs were recovered attributable to *Gudongella* (MAG 2, 98%

completeness, 3% contamination), Acidaminobacteraceae (MAG 3, 100% completeness, 2% contamination), *Acetobacterium* (MAG 4, 98% completeness, 0% contamination), and *Sphaerochaeta halotolerans* (MAG 5, 97% completeness, 0% contamination), which are fermentative and hydrocarbon degrading bacteria encountered in oil and gas settings (Balch et al., 1977; Stams & Hansen, 1984; Grouzdev et al., 2018; Bidzhieva et al., 2018; Wu et al., 2019; Bidzhieva et al., 2020).

A 16S rRNA gene-based survey of the thiosulfate reducing enrichment culture revealed that it was predominantly composed *Desulfomicrobium* (84%), with lower representation of *Dethiosulfovibrio* (7%) and *Desulfuromusa* (7%). All of which are well-characterized groups of sulfate and thiosulfate reducing bacteria that are frequently encountered in oil and gas handling systems (Finster et al., 1997; LaButti et al., 2010; Al Abbas et al., 2013; Islam & Karr, 2013). We obtained three metagenome assembled genomes (MAGs) from the thiosulfate reducing enrichment that were taxonomically identified as *Desulfovibrio ferrophilus* (MAG 6, 93% completeness, 1% contamination), *Syntrophootalea carbonolica* (MAG 7, 99% completeness, 3% contamination), and *Desulfuromonas* (MAG 8, 95% completeness, 0% contamination). The discrepancy in the taxonomic assignment is due to the short reads of the 16S rRNA gene-based survey. Both *Desulfomicrobium* and *Desulfovibrio* fall into the family Desulfomicrobiaceae, so it appears that the *D. ferrophilus*-attributable MAG is the prominent component of the enrichment culture. *D. ferrophilus* was originally isolated from marine sediments under sulfate reducing conditions with Fe⁰ as the sole electron donor and is well-studied for its corrosive activities (Dinh et al., 2004; Chatterjee et al., 2021; Li et al., 2023).

All five MAGs in the cysteine-metabolizing enrichment culture contained genes encoding the cysteine desulhydratase, which degrades cysteine to pyruvate, ammonium, and sulfide (Loddeke et al., 2017; Yokota and Ikeda, 2017; Oguri et al., 2021). While MAGs attributable to *Gudongella* (MAG 2), Acidaminobacteraceae (MAG 3), *Acetobacterium* (MAG 4), and *Sp. halotolerans* (MAG 5) did not include genes encoding phosphate acetyl transferase necessary for pyruvate fermentation to acetate (Table 2-2; Heidelberg et al., 2004), the most prominent component of the enrichment, *D. alaskensis*, contained genes encoding the complete set of enzymes necessary to ferment pyruvate to acetate (Table 2-2). Pyruvate fermentation is common among *Desulfovibrio* (e.g., Tasaki et al., 1993; Meyer et al., 2014), but this metabolism among the Acidaminobacteraceae, *Gudongella*, *Acetobacterium*, and *Sphaerochaeta* is not clear. The MAG attributable to *D. alaskensis* also included genes encoding proteins to assimilate acetate via acetyl-CoA (Table 2-2). For acetate assimilation under these conditions, acetyl-CoA synthetase can convert acetate to acetyl-CoA (with ATP) (Erb, 2011; Tang et al., 2011; Hosmer et al., 2024). The acetyl-CoA can then be reductively carboxylated to pyruvate-by-pyruvate synthase, which can enter a variety of biosynthetic pathways (Erb, 2011; Tang et al., 2011; Hosmer et al., 2024). Acetate assimilation via this pathway is widespread among *Desulfovibrio* spp., *Acetobacterium* spp. and *Spirochaeta* spp. (e.g. Badziong et al., 1979; Ohkuma et al., 2015; Sánchez-Andrea et al., 2020; Shin et al., 2021). Acetate assimilation among *Gudongella* spp. and the Acidaminobacteraceae is not clear. Taken together, it appears that the *D. alaskensis* in the enrichment culture was metabolizing cysteine to

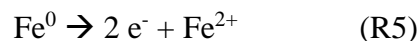
ammonium, sulfide, and pyruvate, obtaining energy via fermentation of pyruvate, and assimilating acetate.

All three MAGs in the thiosulfate enrichment culture contained genes encoding a thiosulfate reductase, which can catalyze the dismutation of thiosulfate to sulfite and sulfide, but only the MAG, attributable to *D. ferrophilus* (MAG 6), contained the sulfite reductase necessary for complete reduction of thiosulfate to sulfide (Haschke and Campbell, 1971; Hatchikian, 1975; Barrett and Clark, 1987; Burns and DiChristina, 2009; Stoffels et al., 2012). Notably, complete sulfate reduction pathways (Qian et al., 2019) were observed in the MAGs attributable to *D. alaskensis* and *D. ferrophilus* (MAGs 1 and 6, respectively). In both enrichment cultures, we were able to capture the most prominent components of our enrichment cultures in our MAGs, and the most abundant components were capable of the targeted metabolisms (cysteine metabolism and thiosulfate reduction).

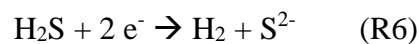
Corrosion under thiol-metabolizing conditions To determine the corrosive activities of the thiol metabolizing enrichment culture, we conducted a series of SC-ZRA incubations. To determine the influence of thiol compounds on corrosion, we carried out incubations with and without the inclusion of cysteine, which served as a model thiol compound. Besides 8 mM cysteine as a substrate, the enrichment medium also included 20 mM acetate as a carbon source, so we sought to determine the influence of a carbon source on the corrosive activities of the thiol-metabolizing enrichment culture. In SC-ZRA incubations with only anoxic synthetic brine (Chinthala et al., 2024), little current was observed, and the potential was approximately 0.7 V throughout the incubations

(Figure 3-1: A and B). Similarly, little current or change of potential were observed in cysteine-free SC-ZRA incubations (Figure 3-1: A and B), and little mass loss was observed from the coupons (Table 2-1). In contrast, positive current was observed in the cysteine-amended incubations (Figure 3-1: A and B), and greater mass loss observed from the WE1 electrode than the WE2 electrode (Table 2-1). This pattern of indicates WE1 served as the anode, WE2 served as the cathode and electron transfer occurred from WE1 to WE2 (Chinthala et al., 2024). These results also indicate that cysteine metabolism was responsible for the observed corrosion. Indeed, sulfur-containing deposits were observed on WE1 (but not WE2) of thiol-containing incubations (Figure 3-2 and 3-3), indicating the role of free sulfide in the corrosive activities observed in these incubations.

While sulfide production appeared to induce electron transfer and corrosion, the direction of electron transfer is inconsistent with the mechanism of corrosion by sulfide depicted in R3. In that case, in the SC-ZRA format, the anodic reaction (R5) would occur on WE2



and the cathodic reaction (R6) would occur on WE1, resulting in negative current (Chinthala et al., 2024).



The current observed in these incubations was positive, and mass loss indicated that WE2 was serving as the cathode, while WE1 was serving as the anode. This inconsistency may be attributable to the sulfide concentration. In previous experiments

(Chinthala et al., 2024), we have observed that with 10 mM sulfide in an SC-ZRA incubation, the current is negative while at lower sulfide concentrations (1 mM), the current is positive. In these cases, the initial accumulation of sulfide appears to cathodically protect the WE that is not exposed to microbiological activity, while corrosion occurs most extensively on the microbe-exposed WE (Chinthala et al., 2024). As such, the kinetics and extents of sulfide accumulation could have influenced the development of anodic and cathodic conditions in these experiments. More broadly, these kinds of sulfide accumulation patterns could influence the localized development of anodic and cathodic regions of metal surfaces.

The inclusion of acetate in the medium enhanced the development of current leading to corrosion when cysteine was present (Figure 3-1: A). While cysteine-derived pyruvate can be fermented to yield energy, acetate is non-fermentable. The acetate can fulfil the carbon requirements of microorganisms. In this case, acetate enhanced corrosion by allowing microorganisms in the enrichment culture to metabolize cysteine-derived pyruvate exclusively as an energetic substrate, while acetate could be used for biomass C, thus enhancing growth and corrosive activities.

Corrosion under thiosulfate-reducing conditions To determine the corrosive activities of the thiosulfate reducing enrichment culture, we conducted a second series of SC-ZRA incubations. To differentiate between MIC via biogenic sulfide (R3) and direct uptake of electrons to support thiosulfate reduction (R4), we incubated the enrichment culture with and without lactate. In SC-ZRA incubations with only anoxic synthetic brine (Chinthala et al., 2024), little current was observed, and the potential was approximately

0.7 V throughout the incubations (Figure 3-4: A and B). In the presence of lactate, thiosulfate was reduced (Figure 3-4: C), potential increased (Figure 3-4: B), and current was negative (Figure 3-4: A), indicating electron transfer from WE2 to WE1. Mass loss from WE2 was greater than WE1 (Table 2-1), indicating that the anodic reaction occurred on WE2, while the cathodic reaction occurred on WE1. WE1 exhibited more pitting corrosion than WE2 in these incubations (Figure 3-6: A and B). These patterns of metabolism, mass loss, current, and potential are consistent with those reported under sulfate reducing conditions by Chinthala et al. (2024) and indicate that the cathodic reaction on WE1 is either supported by biogenic sulfide (R3) or use of Fe⁰ (either directly or indirectly) as an electron donor by the culture coupled to thiosulfate reduction (R4).

Direct extraction of electrons from Fe⁰ may be facilitated by Type IV pili (Deng et al., 2018; Hou et al., 2024), and *D. ferrophilus* has exhibited a capacity to produce conductive extracellular appendages (Deng et al., 2018; Chatterjee et al., 2021). Indeed, Deng et al. (2018) observed the capacity for extracellular electron transfer in *D. ferrophilus*. *D. ferrophilus* has the capacity to produce conductive extracellular appendages, but they may not be involved in direct oxidation of Fe⁰ (Chatterjee et al., 2021; Liang et al., 2021). We were unable to detect genes encoding cytochrome *c*, which are necessary for conductivity in extracellular appendages (Deng et al., 2015; Tsurumaru et al., 2018; Ueki, 2021; Wang et al., 2021; Table 2-2). The pili could facilitate attachment to the metal surface (Hou et al., 2024), whereby Fe⁰ oxidation using H₂ as an intermediate (R3) could occur (Liang et al., 2021). The detection of several genes encoding hydrogenases in the *D. ferrophilus*- and *Sy. carbinolica*-attributable MAGs

support this hypothesis (Table 2-2). Indeed, Liang et al. (2021) indicated that *D. ferrophilus* oxidizes Fe⁰ via oxidation of intermediate H₂ serving as a diffusible electron carrier and not by direct extraction of electrons from Fe⁰.

When lactate was not included in the SC-ZRA incubations, slightly positive current was observed (Figure 3-4: A), and the potential did not reach the same level as in the lactate-amended incubations (Figure 3-4: B). However, thiosulfate depletion was still observed (Figure 3-4: C). This thiosulfate depletion could be attributable to disproportionation, but minimal growth or thiosulfate metabolism were observed in (Fe⁰-free) growth experiments (Figure 3-5: A-C). Growth and thiosulfate reduction were only observed in the presence of lactate (Figure 3-5: A-C). Additionally, genes required for thiosulfate disproportionation were not detected in MAGs from the enrichment culture. These observations indicate that thiosulfate reduction was coupled to oxidation of Fe⁰. However, this proposed activity appears inconsistent with the slightly positive current that we observed. Indeed, mass loss was nearly the same on both WE1 and WE2, and more extensive than we observed in the lactate amended incubations (Table 2-1). Pitting was more extensive on WE1 than WE2 indicating that microbiological Fe⁰ oxidation was occurring on WE1, while homogenous corrosion was occurring on WE2 (Figure 3-6: C and D). Here, competing reactions may have been occurring on the WEs. In previous SC-ZRA incubations, sulfate was used as an electron acceptor, and it is not corrosive abiotically, but in these experiments the thiosulfate itself is corrosive (Marcus and Protopopoff, 1997; Kappes et al., 2012a, 2012b; Choudhary et al., 2015). In the case of the lactate-free incubations, competing cathodic processes (biological on the WE1 side

and abiotic on the WE2 side) could be occurring. On WE1, biological oxidation of Fe⁰ coupled with thiosulfate reduction (R3) is hypothesized to be occurring, with abiotic thiosulfate reduction occurring on WE2 (R7).



The S produced can adsorb on the metal surface (Marcus and Protopopoff, 1997) and may even enhance hydrogen absorption (Kappes, 2012b). The combined effects of hydrogen absorption and metal coverage could then “force” the biological oxidation of Fe⁰ on WE1, while simultaneously corroding WE2, thus resulting in more extensive corrosion. While the current was initially negative in the lactate-amended SC-ZRA incubations, it approached zero later, indicating the possibility of competing reactions limiting current.

Implications for MIC Our results illustrate the utility of ZRA measurements for detecting MIC and the unique patterns of current and corrosion that arise during that process. Both cysteine metabolism and thiosulfate reduction led to patterns that were distinct from those observed under sulfate reducing conditions (Chinthala et al., 2024). Most notably, our observations in the thiosulfate reducing SC-ZRA incubations indicate the influences of competing redox reactions in the contrasting chambers, which mimic the heterogeneous processes on metal surfaces (Miller et al., 2018). The observed current is a sum of the redox processes occurring on WE1 and WE2. Thiosulfate, particularly, may be underappreciated for its role in MIC. Liang et al. (2014) reported that thiosulfate reducing bacteria were the most abundant sulfidogenic bacteria in oil pipeline pigging

sludge, and biocide efficacies may differ between thiosulfate and sulfate reducing bacteria (Crolet, 2005). Our results also illustrate the versatility of microorganisms in oil and gas systems with respect to S metabolism, as cysteine, thiosulfate, and sulfate metabolism, as well as H₂ metabolism and possibly extracellular electron transfer processes (Pieulle et al., 2005; Edwards et al., 2020; Wang et al., 2021; Deng et al., 2015), were widely distributed among our MAGs (Table 2-2).

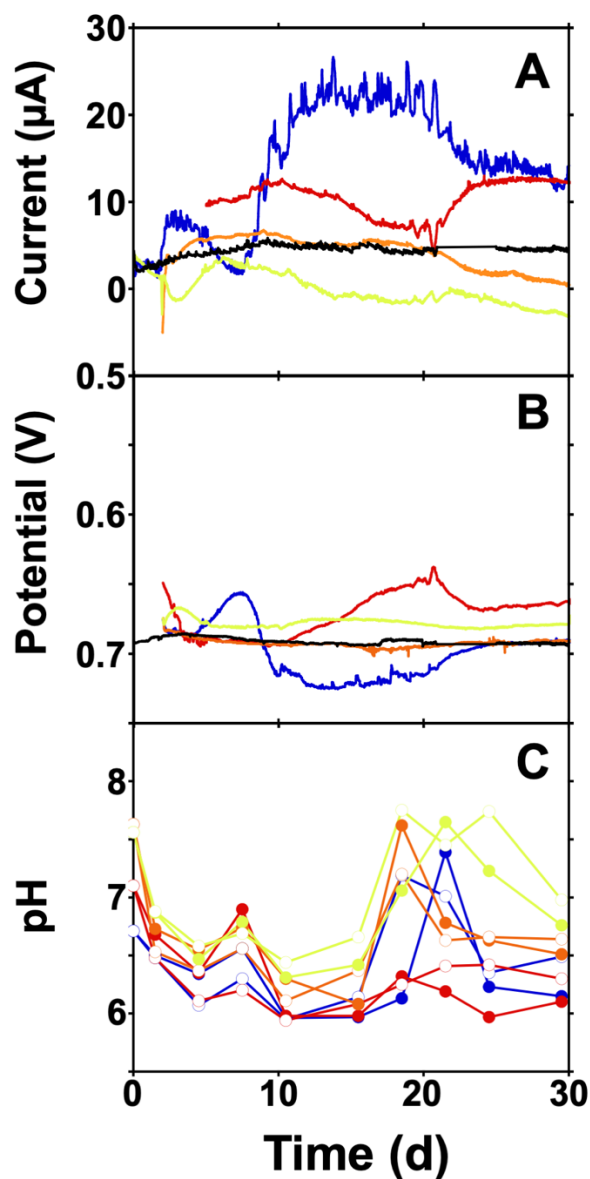


Figure 3-1. Current (A), potential (B), and pH (C) in SC-ZRA incubations that included the cysteine-metabolizing enrichment culture in synthetic brine with both acetate and cysteine amendment (blue), with cysteine amendment only (red), with acetate amendment only (orange), and with neither acetate nor cysteine (yellow). Closed shapes in panels C represent pH concentrations in the WE1 chamber and open shapes represent pH in the WE2 chamber. Current and potential in uninoculated SC-ZRA incubations are shown in black and are from Chinthala et al. (2024).

Table 2-1: Mass loss and predicted mass loss of electrodes in SC-ZRA incubations. The cysteine-metabolizing culture was exposed to variations in acetate and cysteine, while the thiosulfate-reducing culture was tested with and without lactate. Mass loss and corrosion rate ratios were calculated for WE1 and WE2 under each condition. Experimental manipulations for the cysteine-metabolizing culture indicate that the presence or absence of acetate and cysteine influences both the corrosion rate and mass loss, with the highest corrosion rate ratio (2.5) observed in the absence of acetate and the presence of cysteine. In the thiosulfate-reducing culture, the absence of lactate led to an increased mass loss and a corrosion rate ratio near 1.03.

Inoculum	Experimental manipulation	Mass loss (mg) (WE1:WE2)	Corrosion Rate Ratio (WE1:WE2)
Cysteine-metabolizing culture	+Acetate/+cysteine	79:49	1.6
	-Acetate/+cysteine	32:13	2.5
	+Acetate/-cysteine	12:14	0.8
	-Acetate/-cysteine	14:15	0.93
Thiosulfate-reducing culture	+Lactate	32:63	0.5
	-Lactate	91:88	1.03

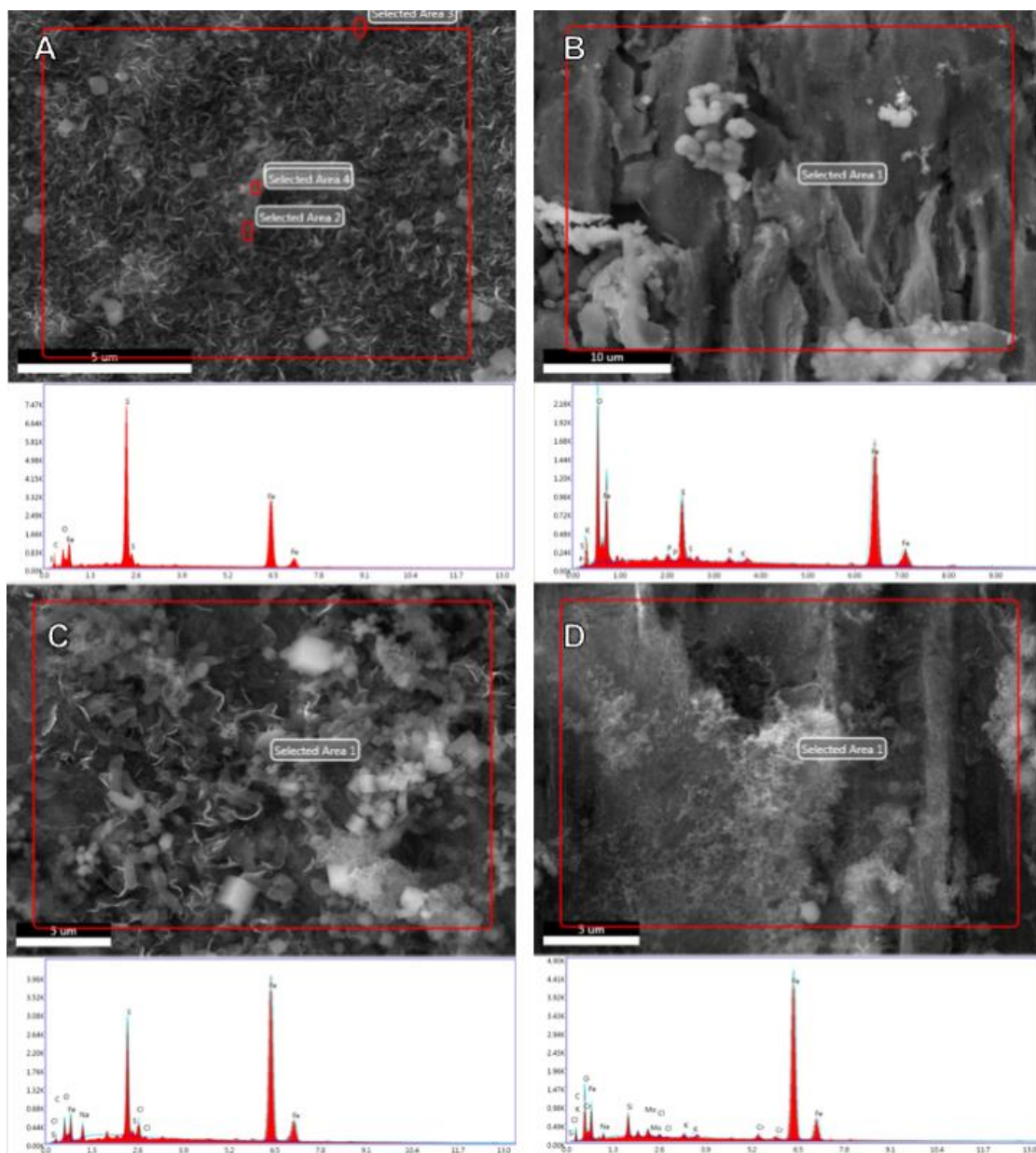


Figure 3-2. Scanning electron micrographs and corresponding EDS spectra (below respective micrographs) of WEs recovered from SC-ZRA incubations with the thiol-metabolizing enrichment culture. Panels A and B are WE1 and WE2, respectively, from an incubation with acetate and cysteine, and panels C and D are WE1 and WE2, respectively, from an incubation with acetate only. The x axis of EDS spectra indicates Energy (keV) and the y axis indicates counts. Scale bars in micrographs in panels A, B, C, and D represent 5 μm , 10 μm , 5 μm , and 5 μm , respectively.

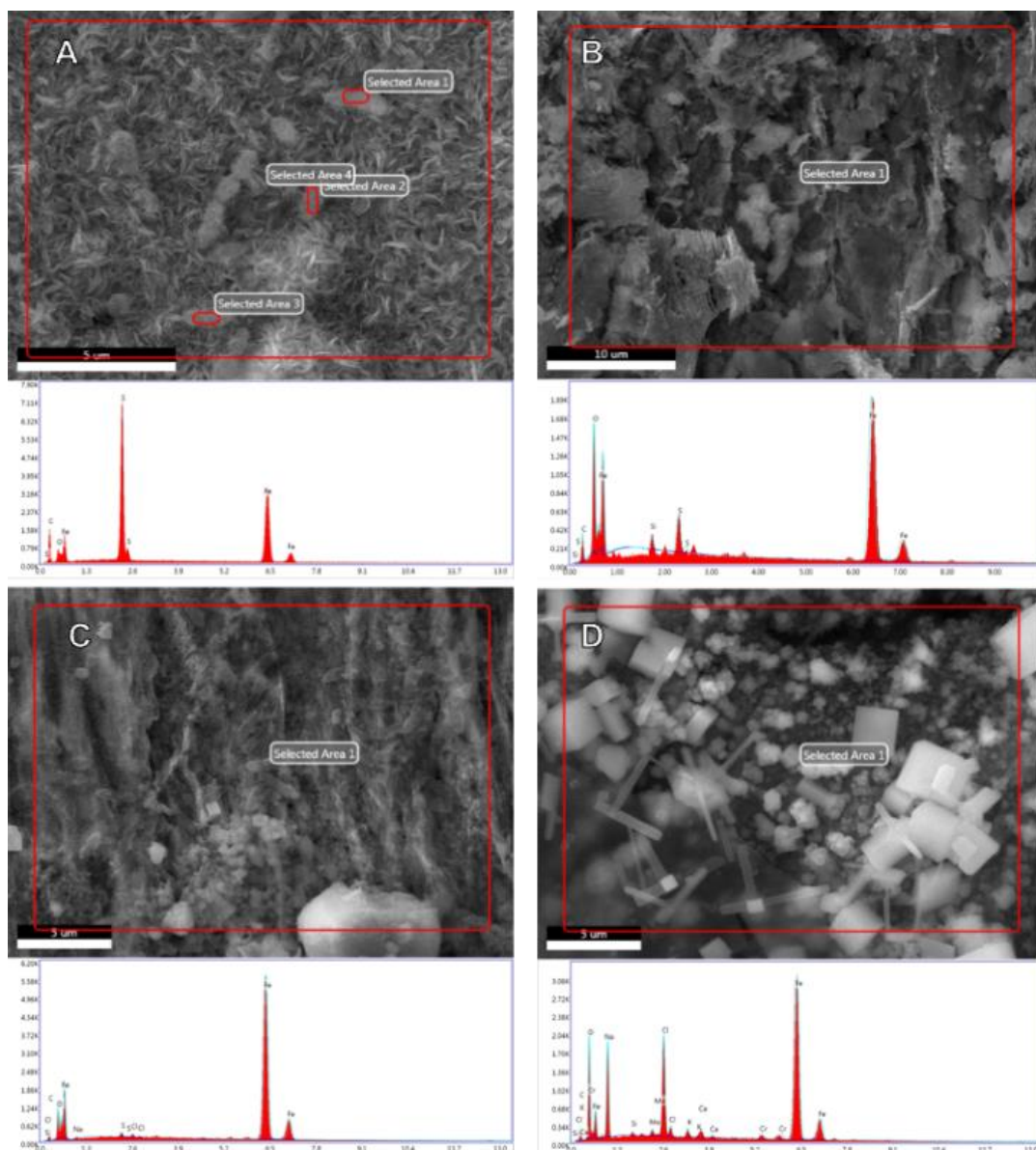


Figure 3-3. Scanning electron micrographs and corresponding EDS spectra (below respective micrographs) of WEs recovered from SC-ZRA incubations with the thiol-metabolizing enrichment culture. Panels A and B are WE1 and WE2, respectively, from an incubation with cysteine, and panels C and D are WE1 and WE2, respectively, from an incubation with no cysteine. The x axis of EDS spectra indicates Energy (keV) and the y axis indicates counts. Scale bars in micrographs in panels A, B, C, and D represent 5 μm, 10 μm, 5 μm, and 5 μm, respectively.

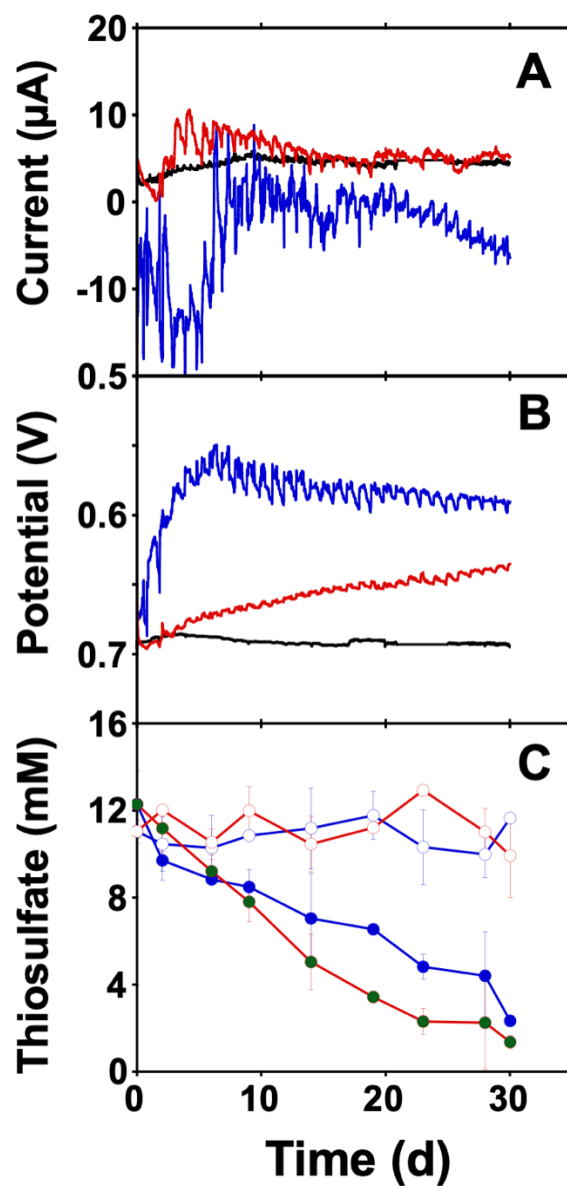


Figure 3-4. Current (A), potential (B), and thiosulfate concentration (C) in SC-ZRA incubations that included the thiosulfate reducing enrichment culture with (blue) and without (red) lactate amendment. Closed shapes in panels C represent thiosulfate concentrations in the WE1 chamber and open shapes represent concentrations in the WE2 chamber. Error bars represent one standard error of duplicate measurements. Current and potential in uninoculated SC-ZRA incubations are shown in black and are from Chinthala et al. (2024).

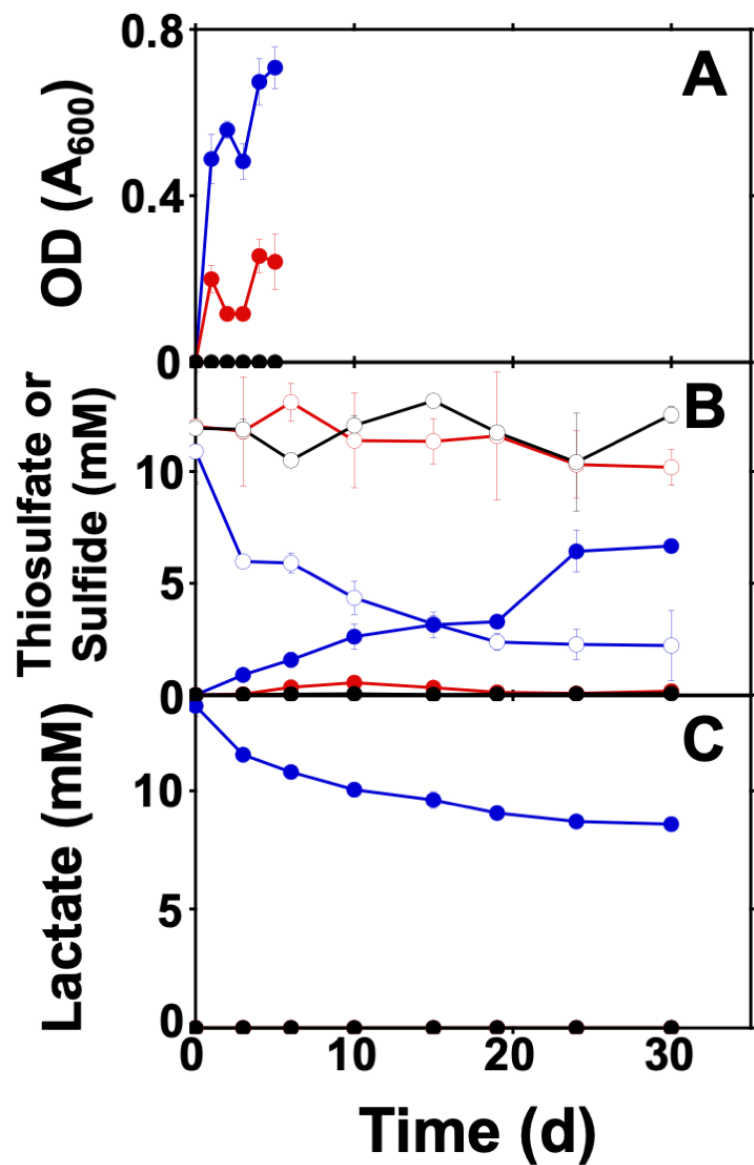


Figure 3-5. Growth (A), thiosulfate (open shapes in B), sulfide (closed shapes in B), and lactate concentrations (C) in uninoculated medium (black), enrichment culture with lactate (blue), and enrichment culture without lactate (red). Error bars represent one standard deviation of triplicate incubations.

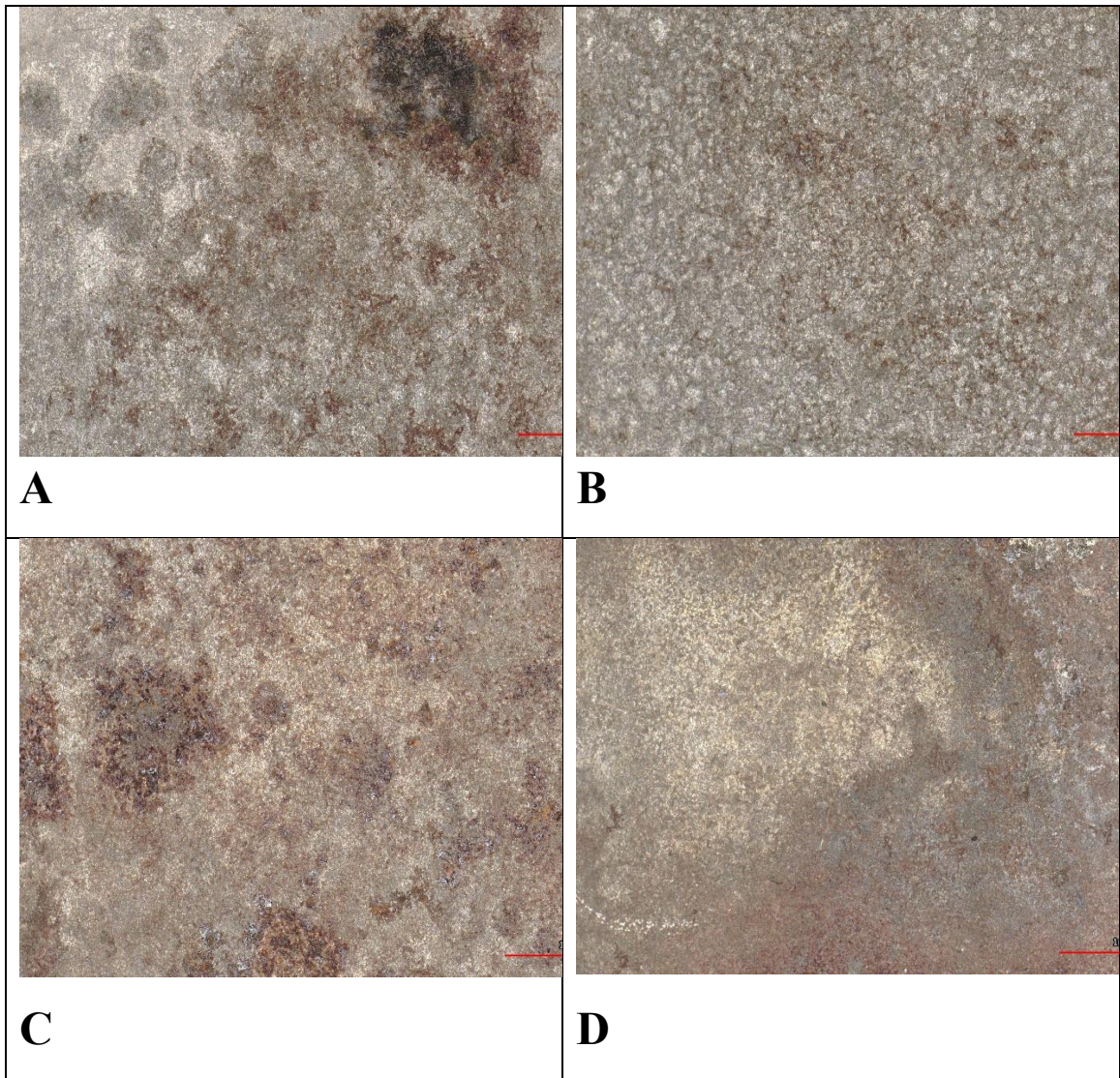


Figure 3-6. Infinite focus microscopy (IFM) images of the thiosulfate ZRA carbon steel coupons recovered from SC-ZRA incubations with the thiosulfate reducing enrichment culture with lactate (WE1 panel A and WE2 panel B) and without lactate (WE1 panel C and WE2 panel D) Thiosulfate without lactate: WE2. Scale bars = 1 mm.

Table 2-2: Genes detected in MAGs recovered from cysteine metabolizing and thiosulfate reducing enrichment cultures.

		Cysteine culture				Thiosulfate culture			
		<i>Desulfovibrio alaskensis</i> (MAG 1)	<i>Giudongella</i> (MAG 2)	Acidaminobacteraceae (MAG 3)	<i>Acetobacterium</i> (MAG 4)	<i>Sphaerochaeta halotolerans</i> (MAG 5)	<i>Desulfovibrio ferrophilus</i> (MAG 6)	<i>Syntrophotalea carbinolica</i> (MAG 7)	<i>Desulfuromonas</i> (MAG 8)
Cysteine degradation	Cysteine desulphydrase	+	+	+	+	+	+	+	+
Pyruvate fermentation	Pyruvate dehydrogenase	+	+	+	+	+	-	+	-
	Pyruvate synthase	+	+	+	+	+	+	+	+
	Phosphate acetyl transferase	+	+	-	-	-	+	-	-
	Acetate kinase	+	+	+	+	+	+	+	+
Acetate assimilation	Acetyl-CoA synthetase	+	-	-	-	-	+	-	-
	Pyruvate synthase	+	+	+	+	+	+	+	+
Thiosulfate reduction	Thiosulfate reductase	+	+	+	-	-	+	-	+
	Thiosulfate reductase (cytochrome)	+	-	-	-	-	+	+	+
	Dissimilatory sulfite reductase	+	-	-	-	-	+	-	-
Sulfate reduction	Sulfate adenylyltransferase	+	-	-	-	-	+	+	+
	Adenylylsulfate reductase	+	-	-	-	-	+	-	-
	Dissimilatory sulfite reductase	+	-	-	-	-	+	-	-
Attachment and/or extracellular electron transport	Type IV Pilus assembly protein PilA	+	-	-	+	-	+	+	-
	Type IV pilus assembly protein PilV	-	-	-	-	-	-	+	-
	Type IV pilus assembly protein PilX	-	-	-	-	-	-	+	+
	Type IV pilus assembly protein PilT	-	+	+	+	-	+	+	+
	Type IV pilus assembly protein PilW	-	-	-	-	-	-	+	+
	Class III cytochrome C family	+	+	-	-	-	-	-	-
	Hydrogenases	NiFe hydrogenase (large and small subunit)	+	-	-	-	-	+	+
	Hydrogenase expression/formation protein F420-non-reducing	+	-	-	-	-	-	-	-
	hydrogenase iron-sulfur subunit	+	-	-	-	-	+	-	-

CHAPTER IV

ENHANCED UNDERSTANDING OF MIC USING INTERDISCIPLINARY APPROACHES

This chapter synthesized the new discoveries made about microbially influenced corrosion (MIC) through the integration of microbiology and electrochemistry. By combining these disciplines, we were able to better understand how microbial processes and electrochemical reactions drove MIC and impacted oil and gas systems.

4.1. Impact of Organic Acid Production by Fermentative Bacteria on Carbon Steel Corrosion

Chapter II investigated how organic acid production by fermentative bacteria from a natural gas pigging pipeline affected carbon steel corrosion. The study tracked glucose depletion, pH reduction, and acetate accumulation during bacterial fermentation. The findings showed that organic acid production lowered the pH, inducing the cathodic reaction of proton reduction to H₂ and causing corrosion on the WE1 side in the SC-ZRA setup. Three metagenome-assembled genomes (MAGs) from *Cytobacillus*, *Lacrimispora*, and *Staphylococcus* spp. were identified, containing genes for fermenting carbohydrates into organic acids, resulting in the acidification of the growth medium. Adding a sodium bicarbonate buffer neutralized the acids, reducing the current generation. This research clarified how microbial activities contributed to corrosion, allowing for the identification

and differentiation of corrosion types. It enabled the monitoring of bacterial fermentative activity and the cathodic reduction of protons, which could damage metallic surfaces.

4.2. Integration of Electrochemistry and Microbiology

The integration of electrochemistry and microbiology expanded our understanding of MIC. Split-cell zero resistance ammetry (SC-ZRA) allowed us to monitor real-time electrochemical processes on metal surfaces, providing insights into how microbial metabolic activities induced corrosion. By using SC-ZRA, we were able to directly measure the current generated by fermentative microbial activity.

Microbiological analyses, including monitoring glucose depletion and acetate accumulation, integrated with metagenomic analysis, indicated that the major components of the enrichment culture were metabolizing glucose via the Emden-Meyerhof-Parnas pathway. This combined approach revealed that the production of organic acids by fermentative bacteria led to a decrease in pH, which in turn induced the reduction of protons to H₂ at the metal surface, causing localized corrosion on the surface of the electrodes. The SC-ZRA setup was crucial for mimicking these small-scale processes, capturing the subtle electrochemical changes that drove corrosion, and providing a detailed understanding that would have been difficult to achieve without this technology.

4.3. Enhanced Understanding and Targeted Mitigation

An interdisciplinary approach allowed us to identify the conditions under which microbial activity accelerated corrosion. For instance, the use of a sodium bicarbonate buffer demonstrated how altering the chemical environment could mitigate microbial corrosion. Understanding the interactions between microbial metabolism and electrochemical processes enabled the development of effective MIC prevention strategies. Some potential methods could be using biocides to target corrosion-causing microbes, optimizing cathodic protection systems, disrupting biofilms to prevent corrosive byproducts, and using chemical inhibitors to block microbial and electrochemical pathways. Sodium bicarbonate could be used as a buffer to neutralize acidic fermentation products and prevent acid-induced corrosion (Gehlbach, 2004). Biocides such as glutaraldehyde effectively reduced bacterial populations in industrial systems, limiting acid production (Sehmi, 2016; Matei, 2020). Cathodic protection might also have been effective in limiting corrosion under acidic conditions (Elsayed, 2022; Silva Campos., et.al 2022). These strategies collectively offered effective protection against the corrosive impact of fermentative bacteria on critical infrastructure. The combination of SC-ZRA and microbiological techniques provided a deeper understanding of MIC and enabled us to monitor and analyze the real-time effects of microbial activity on metal corrosion, identify key metabolic byproducts contributing to corrosion, and explore effective mitigation strategies.

4.4. Roles of Thiol and Thiosulfate Metabolism in Corrosion

Chapter III explored how sulfur-metabolizing bacteria contributed to corrosion in oil and gas pipelines by metabolizing thiosulfate and thiol compounds. We used SC-ZRA to study bacterial enrichments from pigging pipeline sludge, one dominated by *Desulfovibrio alaskensis* for cysteine (used as a model thiol compound) metabolism and another with *Desulfomicrobium* and *Dethiosulfovibrio* for thiosulfate reduction. In thiol metabolism experiments, cysteine degradation produced free sulfide, leading to corrosion, with electrochemical currents highest in the presence of cysteine, particularly when acetate was included as an additional carbon source. For thiosulfate reduction, experiments with and without lactate showed that thiosulfate could drive both biogenic sulfide-mediated MIC and support biological Fe⁰ oxidation, resulting in distinct corrosion patterns. Metagenomic analysis identified genes responsible for sulfate and thiosulfate reduction, thiol degradation, and hydrogenase activity, suggesting that Fe⁰ oxidation might have occurred via H₂ consumption rather than direct electron transfer. These findings underscored the complex roles of microbial metabolism in accelerating corrosion through interactions with metal surfaces in natural gas pipelines.

4.5. Integration of Electrochemistry and Microbiology (2)

The integration of SC-ZRA and microbiology deepened our understanding of how sulfur-metabolizing bacteria contributed to corrosion in oil and gas pipelines. By using SC-ZRA, we were able to track real-time electrochemical changes on metal surfaces, linking these changes to microbial metabolism of thiosulfate and thiol compounds. In our

study, we cultivated bacterial enrichments from pigging pipeline sludge and used SC-ZRA to observe how thiosulfate and thiol metabolism drove corrosion. The thiol-metabolizing culture showed current generation and corrosion when incubated with cysteine, particularly in the presence of acetate, which served as an additional carbon source. These findings aligned with observations of biogenic sulfide-induced corrosion, where cysteine degradation led to free sulfide generation. Similarly, the study of thiosulfate-reducing bacteria revealed that thiosulfate could drive MIC either through biogenic sulfide or direct electron uptake, with lactate enhancing thiosulfate reduction and shifting current patterns. Metagenomic analysis confirmed the presence of genes for sulfate and thiosulfate reduction, thiol degradation, and hydrogenase activity, highlighting the metabolic versatility of these microorganisms in natural gas pipelines. This integration of electrochemistry and microbiology provided an understanding of how microbial metabolism induced localized corrosion, informing targeted mitigation strategies to protect pipeline infrastructure.

4.6. Enhanced Understanding and Targeted Mitigation (2)

The combined use of SC-ZRA and metagenomic characterization allowed us to understand MIC under thiol-metabolizing and thiosulfate reducing conditions. This dual approach enabled the identification of signatures of corrosive microbial activities and their byproducts, leading to the development of targeted mitigation strategies. For example, knowing the metabolic pathways involved in thiosulfate reduction would help in devising inhibitors that could block these pathways, thereby reducing corrosion. Potential inhibitors could include enzyme inhibitors that blocked key enzymes like

thiosulfate reductase, thereby preventing the formation of corrosive byproducts. Enzyme inhibitors like molybdate and tungstate inhibit thiosulfate reductase, thereby preventing the reduction of thiosulfate to corrosive byproducts like sulfide (Zane, 2020). Electron transport chain disruptors such as dinitrophenol and rotenone could limit the energy available for metabolic activities linked to corrosion (Won, 2015; Ozay, 2018; Ichikawa, 2004). Sulfur-binding agents like zinc oxide could sequester corrosive sulfur compounds, effectively neutralizing their impact on metal surfaces (Steudel, 2006, Han, 2017, Joseph, 2015). These strategies might reduce the microbial corrosion of carbon steel in oil and gas systems.

4.7. Future Work

This research represents progress in understanding how microbial activities, particularly those of sulfur-metabolizing and organic acid-producing bacteria, drive MIC in oil and gas systems. However, many avenues remain for further exploration to deepen our knowledge and improve mitigation strategies. Future work should focus on both expanding the mechanistic understanding of MIC and developing practical solutions for corrosion control in industrial environments. While this research has shed light on key microbial metabolic processes that contribute to corrosion, more detailed investigations are required to fully understand the genetic and biochemical pathways involved. Further metagenomic and transcriptomic analyses are needed to identify specific genes and enzymes responsible for corrosion-promoting activities, such as thiosulfate reduction and organic acid production, enabling targeted mitigation strategies. Additionally, studying microbial interactions within biofilms, particularly in mixed-species environments, could

reveal synergistic or antagonistic relationships that influence corrosion rates (Zhao et al., 2023, Jia, 2019). These interactions may affect the rate of substrate utilization and byproduct formation, which are crucial for understanding MIC dynamics (Liamleam & Annachhatre, 2007). Another avenue to explore would be utilizing alternative carbon and sulfur sources. Expanding studies beyond acetate and thiosulfate to explore the use of other organic compounds or sulfur sources that may be present in industrial systems would provide a broader perspective on microbial corrosion mechanisms. Identifying alternative pathways that could drive MIC under different conditions would help anticipate and prevent corrosion in diverse environments.

The use of SC-ZRA has proven effective in real-time monitoring of electrochemical processes associated with MIC. However, additional electrochemical techniques could further refine our understanding and provide complementary data. Future research may explore the use of electrochemical impedance spectroscopy (EIS). EIS can provide more precise, spatially resolved insights into corrosion processes on metal surfaces (Margarit-Mattos, 2020). EIS measures the impedance (resistance to alternating current) of a system, allowing for us to probe the electrochemical properties of metal surfaces and identify corrosion mechanisms (Ikani et al., 2024; Mishra et al., 2020). By combining EIS with SC-ZRA, we could gain a more comprehensive view of the localized corrosion behavior driven by microbial activity, offering both spatial and real-time insights into how corrosion progresses. The integration of SC-ZRA with in-situ surface characterization techniques like scanning electron microscopy (SEM) and atomic force microscopy (AFM) could enable real-time observation of microbial corrosion at the

nanoscale. SEM provides detailed images of surface morphology by scanning a focused electron beam across the sample, while AFM measures surface roughness and topographical changes at the atomic level (Davoodi et al., 2007; Ye et al., 2018; Shen et al., 2024). This combination would allow for the visualization of biofilm formation, surface roughening, and the deposition of corrosive byproducts as they occur, offering deeper insights into microbial corrosion processes.

Guiding Mitigation Strategies

The integration of electrochemistry and microbiology in understanding MIC offers valuable insights for developing targeted detection and mitigation strategies. The use of SC-ZRA allows for the real-time monitoring of microbial metabolic activities and their electrochemical effects on metal surfaces. By linking specific microbial pathways, such as organic acid production or sulfur metabolism, to electrochemical changes, it becomes possible to predict when and where MIC is most likely to occur.

Detection strategies could involve monitoring the metabolic byproducts of microbes that drive corrosion, such as organic acids from fermentative bacteria or sulfides from sulfur-metabolizing organisms. For example, real-time electrochemical sensing technologies like SC-ZRA, combined with metagenomic analysis, could be employed to detect early signs of these corrosive byproducts. This would allow technicians to identify high-risk environments before significant corrosion occurs. Additionally, understanding microbial signatures could help refine microbial monitoring programs by focusing on specific genera or species known to accelerate corrosion.

Mitigation strategies could be tailored to disrupt microbial pathways linked to corrosion. For instance, the research highlights the effectiveness of sodium bicarbonate in neutralizing acidic byproducts from fermentative bacteria, thereby mitigating corrosion. Similarly, enzyme inhibitors that block key steps in sulfur metabolism, such as thiosulfate reduction, could prevent the formation of corrosive compounds like sulfide. Biocides could be used to selectively target corrosive microbial communities, while alternative strategies like cathodic protection could address electrochemical imbalances created by microbial activity(Videla, 2002; Jia et al., 2019). Combining these approaches would offer a comprehensive solution for preventing MIC in oil and gas systems.

4.8. Supplemental Information

<u>Metabolic Current Ranking</u> *Based on Peak Current			
<u>Ranking (Highest- Lowest)</u>	<u>SC-ZRA Run/Metabolism</u>	<u>Peak Current (μA)</u>	<u>Corrosion Rate Ratio/ Mass Loss(mg) (WE1:WE2)</u>
1	Thiol (+Acetate, +Cysteine)	25	1.6 (79:49)
2	Thiol (-Acetate, +Cysteine)	12	2.5 (32:13)
3	Thiosulfate (-Lactate)	10	1.03 (91:88)
4	Fermenter (Control with Bicarbonate)	7	1.0 (35:35)
5	Thiol (+Acetate, -Cysteine)	5	0.8 (12:14)
6	Fermenter (Control with No Bicarbonate)	3	0.9 (38:42)
7	Thiol (-Acetate, -Cysteine)	2	0.93 (14:15)
8	Thiosulfate (+Lactate)	1	0.5 (32:63)
9	Fermenter (Live with Bicarbonate)	-3	1.3 (42:32)
10	Fermenter (Live with No Bicarbonate)	-12	0.5 (13:26)

Synthesis of Current Magnitudes and Mechanism

The table presents a comparative analysis of peak current magnitudes from SC-ZRA runs involving three distinct metabolic processes: thiosulfate reduction, thiol

metabolism, and fermentative acid production. The data revealed notable trends in both the magnitude and direction of the electrochemical currents, which can be linked to the metabolic pathways driving corrosion.

Thiol Metabolism

The highest peak current, 25 μA , was recorded in the thiol metabolism run with both acetate and cysteine present, yielding a corrosion rate ratio (CRR) of 1.6 (79:49). This suggests that the combined availability of a carbon source (*acetate*) and a sulfur source (*cysteine*) accelerated corrosion, likely due to the increased production of biogenic sulfide, which enhanced electrochemical activity on the metal surface. When acetate was removed, leaving only cysteine, the peak current decreased to 12 μA , but the CRR increased to 2.5 (32:13), indicating more localized corrosion at WE1. This pattern suggested that, although the absence of acetate may reduce biofilm growth, the presence of cysteine alone drives significant sulfide production, leading to focused corrosion at the anode. In the absence of cysteine, currents were further reduced, with the acetate-only condition generating a peak current of 5 μA and a CRR of 0.8 (12:14). This decrease reflects the absence of sulfur-driven corrosion, as cysteine is a key sulfur source for generating corrosive byproducts in thiol metabolism.

Thiosulfate Reduction

In the presence of lactate, thiosulfate reduction produced the lowest peak current, just 1 μA , with a CRR of 0.5 (32:63), suggesting limited corrosion dominated by cathodic activity on WE2. The reduction in current may be due to the inefficiency of the

thiosulfate reduction pathway when utilizing lactate, potentially hindering corrosion processes.

When lactate was absent, the peak current increased to 10 μA , and the CRR balanced at 1.03 (91:88), indicating a more even distribution of corrosion between WE1 and WE2. This suggests that in the absence of lactate, thiosulfate-reducing bacteria operate more efficiently, likely generating more corrosive byproducts like sulfide, which enhance electron transfer and accelerate corrosion.

Fermentative Metabolism

Under control conditions with bicarbonate as a pH buffer, currents were relatively low, at 7 μA and 3 μA , with near-neutral CRRs of 1.0 and 0.9, respectively. The bicarbonate neutralized the organic acids produced by fermentation, thereby mitigating corrosion. In contrast, fermentative conditions without bicarbonate buffering exhibited the most negative currents, with peak values of -3 μA and -12 μA , along with lower CRRs of 1.3 and 0.5. These negative currents indicate cathodic dominance on WE1, reflecting conditions where organic acid production drives localized pH reduction, but the absence of buffering limits extensive corrosion.

Trends in Current Magnitudes and Direction

Thiol metabolism consistently generated the highest peak currents, indicating that sulfur metabolism (*particularly in the presence of cysteine*) is a major driver of MIC. Thiosulfate reduction produced moderate currents, with lactate not producing as much

current as the lactate free incubation. This suggests a balance between biotic and abiotic corrosion depending on electron donors (*i.e.*, *lactate*) and sulfur sources (*thiosulfate*). Fermentative metabolism, particularly under buffered conditions, tends to result in low or negative currents, reflecting minimal corrosion or even cathodic protection.

Corrosion Rate Ratios

The corrosion rate ratios (CRRs) aligned with the current magnitudes. Higher currents correspond to increased mass loss on WE1 (anode), particularly in thiol (+*acetate*, +*cysteine*) conditions, where the highest CRR of 1.6 (79:49) occurs. Conversely, the negative currents in fermenter conditions without bicarbonate correlate with lower mass loss on WE1 compared to WE2, as evidenced by the 0.5 (13:26) CRR. These trends illustrate how microbial metabolism, substrate availability, and environmental conditions (*i.e.*, *pH buffering*) influence both the direction and magnitude of MIC, offering valuable insights for mitigation strategies.

4.9. Conclusions

The integration of electrochemistry and microbiology advanced our understanding of MIC across all three projects discussed in this dissertation. Each project combined insights from both fields to explore how microbial activity accelerates corrosion. By using the SC-ZRA technique, we were able to track real-time electrochemical changes on metal surfaces, offering precise measurements of the corrosion processes influenced by microbial activity. This technology enabled us to monitor shifts in current, such as those

driven by organic acid production in fermentative bacteria or thiosulfate and thiol metabolism by sulfur-metabolizing bacteria.

Additionally, metagenomic analyses deepened our understanding by identifying the genetic and enzymatic drivers behind these microbial processes. For example, the identification of genes responsible for carbohydrate fermentation and organic acid production helped to pinpoint the exact microbial activities that led to corrosion in carbon steel systems. Similarly, the discovery of genes linked to thiosulfate reduction and cysteine degradation in sulfur-metabolizing bacteria illustrated the diversity of microbial metabolic pathways contributing to MIC. These projects shared a common theme of illustrating the interaction between microbial metabolic byproducts and electrochemical processes that drive corrosion. In the case of fermentative bacteria, the production of organic acids lowered the pH, inducing localized corrosion through proton reduction. For sulfur-metabolizing bacteria, free sulfide production from cysteine degradation or thiosulfate reduction facilitated biofilm formation and accelerated corrosion.

By combining SC-ZRA with metagenomics, we were able to uncover electrochemical mechanisms behind MIC and link them to specific microbial pathways. This interdisciplinary approach was instrumental in identifying potential mitigation strategies, including buffering agents, biocides, and enzyme inhibitors that target the metabolic activities responsible for corrosion. Ultimately, integrating electrochemistry and microbiology enabled a comprehensive analysis of MIC, equipping us with both mechanistic insights and practical solutions for corrosion control in oil and gas pipelines.

REFERENCES

- Al Abbas, F. M., Bhola, R., Spear, J. R., Olson, D. L., & Mishra, B. (2013). Electrochemical Characterization of Microbiologically Influenced Corrosion on Line pipe Steel Exposed to Facultative Anaerobic *Desulfovibrio* sp. *International Journal of Electrochemical Science*, 8(1), 859–871.
[https://doi.org/https://doi.org/10.1016/S1452-3981\(23\)14063-6](https://doi.org/10.1016/S1452-3981(23)14063-6)
- Alley, B., Beebe, A., Rodgers, J., Jr, & Castle, J. W. (2011). Chemical and physical characterization of produced waters from conventional and unconventional fossil fuel resources. *Chemosphere* **85**, 74–82.
<https://doi.org/10.1016/j.chemosphere.2011.05.043>
- Amir, A., McDonald, D., Navas-Molina, J. A., Kopylova, E., Morton, J. T., Zech Xu, Z., Kightley, E. P., Thompson, L. R., Hyde, E. R., Gonzalez, A., & Knight, R. (2017). Deblur rapidly resolves single-nucleotide community sequence patterns. *mSystems* **2**, e00191-16. <https://doi.org/10.1128/mSystems.00191-16>
- Arkin AP, Cottingham RW, Henry CS, Harris NL, Stevens RL, Maslov S, et al. KBase: The United States Department of Energy Systems Biology Knowledgebase. *Nature Biotechnology*. 2018;36: 566. doi: 10.1038/nbt.4163

Arkin, A. P., Cottingham, R. W., Henry, C. S., Harris, N. L., Stevens, R. L., Maslov, S., Dehal, P., Ware, D., Perez, F., Canon, S., Sneddon, M. W., Henderson, M. L., Riehl, W. J., Murphy-Olson, D., Chan, S. Y., Kamimura, R. T., Kumari, S., Drake, M. M., Brettin, T. S., Glass, E. M., Chivian, D., Gunter, D., Weston, D. J., Allen, B. H., Baumohl, J. Best, A. A., Bowen, B., Brenner, S. E., Bun, C. C., Chandonia, J.-M., Chia, J.-M., Colasanti, R., Conrad, N., Davis, J. J., Davison, B. H., DeJohgh, M., Devoid, M., Dietrich, E., Dubchak, I., Edirisinghe, J. N., Fang, G., Faria, J. P., Frybarger, P. M., Gerlach, W., Gerstein, M., Anette, Greiner, Gurtowski, J., Haun, H. L., He, F., Jain, R., Joachimiak, M. P., Keegan, K. P., Kondo, S., Kumar, V., Land, M. L., Meyer, F., Mills, M., Novichkov, P. S., Oh, T., Olsen, G. J., Olson, R., Parello, B., Pasternak, S., Pearson, E., Poon, S. S., Price, G. A., Ramakrishan, S., Ranjan, P., Ronald, P. C., Schatz, M. C., Seaver, S. M. D., Shukla, M., Sutormin, R. A., Syed, M. H., Thomason, J., Tintle, N. L., Wang, D., Xia, F., Yoo, H., Yoo, S., & Yu, D. (2018). KBase: The United States Department of Energy Systems Biology Knowledgebase. *Nat. Biotechnol.* **36**, 566–569. <https://doi.org/10.1038/nbt.4163>

ASTM International. (2011). Standard practice for preparing, cleaning, and evaluating corrosion test specimens. ASTM G1-03. ASTM International, West Conshohocken, PA.

ASTM International. (2014). Standard guide for electrolytic polishing of metallographic specimens. ASTM E1558-09. ASTM International, West Conshohocken, PA.

- Babu, B., Maruthamuthu, S., Rajasekar, A., Nagu, M., & Palaniswamy, N. (2006). Microbiologically influenced corrosion in dairy effluent. *Int. J. Environ. Sci. Technol.* **3**, 159-166. <https://doi.org/10.1007/BF03325920>
- Badziong, W.D., Ditter, B., & Thauer, R.K. (1979). Acetate and carbon dioxide assimilation by *Desulfovibrio vulgaris* (Marburg), growing on hydrogen and sulfate as sole energy source. *Archives of Microbiology*, **123**, 301-305.
- Balch, W. E., Schoberth, S., Tanner, R. S., & Wolfe, R. S. (1977). *Acetobacterium*, a new genus of hydrogen-oxidizing, carbon dioxide-reducing, anaerobic bacteria. *International Journal of Systematic and Evolutionary Microbiology*, **27**(4), 355–361. <https://doi.org/10.1099/00207713-27-4-355>
- Baranwal, P. K., & Rajaraman, P. V. (2019). Electrochemical investigation on effect of sodium thiosulfate (Na₂S₂O₃) and ammonium chloride (NH₄Cl) on carbon steel corrosion. *Journal of Materials Research and Technology*, **8**(1), 1366–1378. <https://doi.org/https://doi.org/10.1016/j.jmrt.2018.05.029>
- Barrett, E. L., & Clark, M. A. (1987). Tetrathionate reduction and production of hydrogen sulfide from thiosulfate. *Microbiological reviews*, **51**(2), 192–205. <https://doi.org/10.1128/mr.51.2.192-205.1987>
- Bidzhieva, S. K., Sokolova, D. S., Grouzdev, D. S., Kostrikina, N. A., Poltarau, A. B., Tourova, T. P., Shcherbakova, V. A., Troshina, O. Y., & Nazina, T. N. (2020). *Sphaerochaeta halotolerans* sp. nov., a novel spherical halotolerant spirochete from a Russian heavy oil reservoir, emended description of the

genus *Sphaerochaeta*, reclassification of *Sphaerochaeta coccooides* to a new genus *Parasphaerochaeta* gen. nov. as *Parasphaerochaeta coccooides* comb. nov. and proposal of *Sphaerochaetaceae* fam. nov. *International journal of systematic and evolutionary microbiology*, 70(8), 4748–4759.

<https://doi.org/10.1099/ijsem.0.004340>

Bidzhieva, S.K., Sokolova, D.S., Tourova, T.P. *et al.* Bacteria of the Genus *Sphaerochaeta* from Low-Temperature Heavy Oil Reservoirs (Russia). *Microbiology* **87**, 757–765 (2018).

<https://doi.org/10.1134/S0026261718060048>

Biwer, P., Neumann-Schaal, M., Henke, P., Jahn, D., & Schulz, S. (2022). Thiol Metabolism and Volatile Metabolome of *Clostridioides difficile*. *Frontiers in microbiology*, 13, 864587. <https://doi.org/10.3389/fmicb.2022.864587>

Bocian-Ostrzycka, K. M., Grzeszczuk, M. J., Banaś, A. M., & Jagusztyn-Krynicka, E. K. (2017). Bacterial thiol oxidoreductases - from basic research to new antibacterial strategies. *Applied microbiology and biotechnology*, 101(10), 3977–3989.

<https://doi.org/10.1007/s00253-017-8291-8>

Boden, R., & Hutt, L. P. (2019). *Bacterial Metabolism of C1 Sulfur Compounds BT - Aerobic Utilization of Hydrocarbons, Oils, and Lipids* (F. Rojo (ed.); pp. 421–463). Springer International Publishing. https://doi.org/10.1007/978-3-319-50418-6_9

Bokulich, N. A., Subramanian, S., Faith, J. J., Gevers, D., Gordon, J. I., Knight, R., Mills, D. A., & Caporaso, J. G. (2013). Quality-filtering vastly improves diversity

estimates from Illumina amplicon sequencing. *Nat. Meth.***10**, 57–59.

<https://doi.org/10.1038/nmeth.2276>

Bokulich, N. A., Kaehler, B. D., Rideout, J. R., Dillon, M., Bolyen, E., Knight, R., ... Caporaso, J. G. (2018). Optimizing taxonomic classification of marker-gene amplicon sequences with QIIME 2's q2-feature-classifier plugin. *Microbiome* **6**, 90. doi: 10.1186/s40168-018-0470-z.

Bolger, A. M., Lohse, M., & Usadel, B. (2014). Trimmomatic: a flexible trimmer for Illumina sequence data. *Bioinformatics* **30**, 2114–2120.

<https://doi.org/10.1093/bioinformatics/btu170>

Bolyen, E., Rideout, J. R., Dillon, M. R., Bokulich, N. A., Abnet, C. C., Al-Ghalith, G. A., Caporaso, J. G. (2019). Reproducible, interactive, scalable and extensible microbiome data science using QIIME 2. *Nat. Biotechnol.* **37**, 852–857. doi: 10.1038/s41587-019-0209-9.

Brown, B., Brown, S., & Senko, J. (2012). Microbial communities associated with wet flue gas desulfurization systems. *Front. Microbiol.* **3**, 412.

<https://www.frontiersin.org/articles/10.3389/fmicb.2012.00412>

Burns, J. L., & DiChristina, T. J. (2009). Anaerobic respiration of elemental sulfur and thiosulfate by *Shewanella oneidensis* MR-1 requires *psrA*, a homolog of the *phsA* gene of *Salmonella enterica* serovar typhimurium LT2. *Applied and environmental microbiology*, **75**(16), 5209–5217.

<https://doi.org/10.1128/AEM.00888-09>

- Caporaso, J. G., Lauber, C. L., Costello, E. K., Berg-Lyons, D., Gonzalez, A., Stombaugh, J., Knights, D., Gajer, P., Ravel, J., Fierer, N., Gordon, J. I., & Knight, R. (2011). Moving pictures of the human microbiome. *Genome biology*, *12*(5), R50. <https://doi.org/10.1186/gb-2011-12-5-r50>
- Caporaso, J. G., Lauber, C. L., Walters, W. A., Berg-Lyons, D., Lozupone, C. A., Turnbaugh, P. J., Fierer, N., & Knight, R. (2011). Global patterns of 16S rRNA diversity at a depth of millions of sequences per sample. *Proc. Nat. Acad. Sci. USA* **108**, 4516–4522. <https://doi.org/10.1073/pnas.1000080107>
- Chatterjee, M., Fan, Y., Cao, F., Jones, A. A., Pilloni, G., & Zhang, X. (2021). Proteomic study of *Desulfovibrio ferrophilus* IS5 reveals overexpressed extracellular multi-heme cytochrome associated with severe microbiologically influenced corrosion. *Scientific reports*, *11*(1), 15458. <https://doi.org/10.1038/s41598-021-95060-0>
- Chaumeil, P. A., Mussig, A. J., Hugenholtz, P., & Parks, D. H. (2019). GTDB-Tk: a toolkit to classify genomes with the Genome Taxonomy Database. *Bioinformatics* **36**, 1925–1927. <https://doi.org/10.1093/bioinformatics/btz848>
- Chinthala, S. P., Sadek, A., Davis, J., Senko, J. M., & Monty, C. N. (2023). Real-time electrochemical monitoring of the progress of sulfate reducing bacterially–induced corrosion of carbon steel. *Corrosion* 4415. <https://doi.org/10.5006/4415>

- Choudhary, L., Macdonald, D. D., & Alfantazi, A. (2015). Role of Thiosulfate in the Corrosion of Steels: A Review. *Corrosion*, *71*(9), 1147–1168.
<https://doi.org/10.5006/1709>
- Crolet, J.-L. (2005). Microbial Corrosion in the Oil Industry: A Corrosionist's View. In *Petroleum Microbiology* (pp. 143–169).
<https://doi.org/https://doi.org/10.1128/9781555817589.ch8>
- Davidova, I. A., Duncan, K. E., Perez-Ibarra, B. M., & Suflita, J. M. (2012). Involvement of thermophilic archaea in the biocorrosion of oil pipelines. *Environ. Microbiol.* **14**, 1762–1771. <https://doi.org/https://doi.org/10.1111/j.1462-2920.2012.02721.x>
- de Paula Cosmo, R., de Assis Ressel Pereira, F., Soares, E. J., & Leibsohn Martins, A. (2022). Modeling and validation of the CO₂ degassing effect on CaCO₃ precipitation using oilfield data. *Fuel* **310**, 122067.
<https://doi.org/https://doi.org/10.1016/j.fuel.2021.122067>
- de Sousa, V. S., da-Silva, A. P. S., Sorenson, L., Paschoal, R. P., Rabello, R. F., Campana, E. H., Pinheiro, M. S., Dos Santos, L. O. F., Martins, N., Botelho, A. C. N., Picão, R. C., Fracalanza, S. E. L., Riley, L. W., Sensabaugh, G., & Moreira, B. M. (2017). *Staphylococcus saprophyticus* recovered from humans, food, and recreational waters in Rio de Janeiro, Brazil. *Int. J. Microbiol.* **2017**, 4287547.
<https://doi.org/10.1155/2017/4287547>
- Deng, X., Dohmae, N., Neelson, K. H., Hashimoto, K., & Okamoto, A. (2018). Multi-heme cytochromes provide a pathway for survival in energy-limited

environments. *Science Advances*, 4(2), eaao5682.

<https://doi.org/10.1126/sciadv.aao5682>

Deng, X., Nakamura, R., Hashimoto, K., & Okamoto, A. (2015). Electron Extraction from an Extracellular Electrode by *Desulfovibrio ferrophilus* Strain IS5 Without Using Hydrogen as an Electron Carrier. *Electrochemistry*, 83(7), 529–531.

<https://doi.org/10.5796/electrochemistry.83.529>

Di Franco, F., Tranchida, G., Pupillo, D., Gherzi, G., Cinà, P., Virtanen, S., & Santamaria, M. (2021). Effect of E. coli biofilm formation and removal on passive films on AISI 316L during fermentation processes. *Corr. Sci.* **185**, 109430.

<https://doi.org/https://doi.org/10.1016/j.corsci.2021.109430>

Dinh, H. T., Kuever, J., Mussmann, M., Hassel, A. W., Stratmann, M., & Widdel, F. (2004). Iron corrosion by novel anaerobic microorganisms. *Nature*, 427(6977), 829–832. <https://doi.org/10.1038/nature02321>

Duncan, K. E., Gieg, L. M., Parisi, V. A., Tanner, R. S., Tringe, S. G., Bristow, J., & Suflita, J. M. (2009). Biocorrosive thermophilic microbial communities in Alaskan North Slope oil facilities. *Environmental Science and Technology*, 43(20), 7977–7984. <https://doi.org/10.1021/es9013932>

Edwards, A. M., Addo, M. A., & Dos Santos, P. C. (2021). tRNA Modifications as a Readout of S and Fe-S Metabolism. *Methods in molecular biology (Clifton, N.J.)*, 2353, 137–154. https://doi.org/10.1007/978-1-0716-1605-5_8

Elsayed, A., Nofal, A., & Attia, G. (2022). Development of metal oxide incorporated Al-Zn-Sn sacrificial anodes processed by stir casting and heat treatment. *Journal of*

Solid-State Electrochemistry, 26(12), 2659–2672. <https://doi.org/10.1007/s10008-022-05251-6>

Emam, E., Moawad, T. M., & Aboul-Gheit, N. (2014). Evaluating the characteristics of offshore oilfield produced water. *Petrol. Coal* **56**, 363–372.

Enning, D., & Garrelfs, J. (2014). Corrosion of Iron by Sulfate-Reducing Bacteria: New Views of an Old Problem. *Applied and Environmental Microbiology*, 80(4), 1226 LP – 1236. <http://aem.asm.org/content/80/4/1226.abstract>

Erb T. J. (2011). Carboxylases in natural and synthetic microbial pathways. *Applied and environmental microbiology*, 77(24), 8466–8477.
<https://doi.org/10.1128/AEM.05702-11>

Feio, M., Zinkevich, V., Beech, I., Llobet-Brossa, E., Eaton, P., Schmitt, J., & Guezennec, J. (2004). *Desulfovibrio alaskensis* sp. nov., a sulphate-reducing bacterium from a soured oil reservoir. *International Journal of Systematic and Evolutionary Microbiology*, 54, 1747–1752. <https://doi.org/10.1099/ijs.0.63118-0>

Finster, K., Coates, J., Liesack, W., & Pfennig, N. (1997). *Desulfuromonas thiophila* sp. nov., a New Obligately Sulfur-Reducing Bacterium from Anoxic Freshwater Sediment. *International Journal of Systematic Bacteriology*, 47, 754–758.
<https://doi.org/10.1099/00207713-47-3-754>

Flemming, H. C. (1996). Biofouling and microbiologically influenced corrosion (MIC)- An Economic and Technical Overview., *Microbial Deterioration of Materials*. 5-14.

- Gajda, I., Greenman, J., & Ieropoulos, I. A. (2018). Recent advancements in real-world microbial fuel cell applications. *Current Opinion in Electrochemistry*, *11*, 78–83. <https://doi.org/https://doi.org/10.1016/j.coelec.2018.09.006>
- Gehlbach, B. K., & Schmidt, G. A. (2004). Bench-to-bedside review: treating acid-base abnormalities in the intensive care unit - the role of buffers. *Critical care (London, England)*, *8*(4), 259–265. <https://doi.org/10.1186/cc2865>
- Gerken, T., Wiegner, T. N., & Economy, L. M. (2022). A comparison of soil *Staphylococcus aureus* and fecal indicator bacteria concentrations across land uses in a Hawaiian watershed. *J. Environ. Qual.* **51**, 916–929. <https://doi.org/10.1002/jeq2.20380>
- Giai, C., Rincón Ortiz, M., Kappes, M., Senko, J., & Iannuzzi, M. (2016). Efficacy of sterilization methods and their influence on the electrochemical behavior of plain carbon steel. *J. Electrochem. Soc.* **163**, C633–C642. <https://doi.org/10.1149/2.0271610jes>
- Gieg, L. M., Fowler, S. J., & Berdugo-Clavijo, C. (2014). Syntrophic biodegradation of hydrocarbon contaminants. *Curr. Opin. Biotechnol.* **27**, 21–29. <https://doi.org/10.1016/j.copbio.2013.09.002>
- Grouzdev D. S., Rysina M. S., Bryantseva I. A., Gorlenko V. M., Gaisin V. A. (2018). Draft genome sequences of “Candidatus Chloroploca asiatica” and “Candidatus Viridilinea mediisalina”, candidate representatives of the Chloroflexales order: phylogenetic and taxonomic implications. *Stand. Genomic Sci.* *13*:24. doi: 10.1186/s40793-018-0329-8

- Gu, T. (2014). Theoretical modeling of the possibility of acid producing bacteria causing fast pitting biocorrosion. *J. Microbial Biochem. Technol.* **6**, 067-073.
<https://doi.org/10.4172/1948-5948.1000124>
- Guan, F., Zhai, X., Duan, J., Zhang, M., & Hou, B. (2016). Influence of Sulfate-Reducing Bacteria on the Corrosion Behavior of High Strength Steel EQ70 under Cathodic Polarization. *PLOS ONE*, *11*, e0162315.
<https://doi.org/10.1371/journal.pone.0162315>
- Haendiges, J., González-Escalona, N., Timme, R., & Balkey, M. (2020). Illumina DNA Prep (M) Tagmentation Library Preparation for use on an Illumina MiSeq Sequencer v1. <https://doi.org/10.17504/protocols.io.bcbnisme>
- Han, J., Liu, W., Zhang, T., Xue, K., Li, W., Jiao, F., & Qin, W. (2017). Mechanism study on the sulfidation of ZnO with sulfur and iron oxide at high temperature. *Scientific Reports*, *7*(1), 42536. <https://doi.org/10.1038/srep42536>
- Haschke, R. H., & Campbell, L. L. (1971). Thiosulfate reductase of *Desulfovibrio vulgaris*. *Journal of bacteriology*, *106*(2), 603–607.
<https://doi.org/10.1128/jb.106.2.603-607.1971>
- Hatchikian E. C. (1975). Purification and properties of thiosulfate reductase from *Desulfovibrio gigas*. *Archives of microbiology*, *105*(3), 249–256.
<https://doi.org/10.1007/BF00447143>
- Heidelberg, J. F., Seshadri, R., Haveman, S. A., Hemme, C. L., Paulsen, I. T., Kolonay, J. F., Eisen, J. A., Ward, N., Methe, B., Brinkac, L. M., Daugherty, S. C., Deboy, R. T., Dodson, R. J., Durkin, A. S., Madupu, R., Nelson, W. C., Sullivan, S. A.,

- Fouts, D., Haft, D. H., ... Fraser, C. M. (2004). The genome sequence of the anaerobic, sulfate-reducing bacterium *Desulfovibrio vulgaris* Hildenborough. *Nature Biotechnology*, 22(5), 554–559. <https://doi.org/10.1038/nbt959>
- Hosmer, J., McEwan, A. G., & Kappler, U. (2024). Bacterial acetate metabolism and its influence on human epithelia. *Emerging Topics in Life Sciences*, 8(1), 1–13. <https://doi.org/https://doi.org/10.1042/ETLS20220092>
- Hou, L., Cortez, R., Hagerman, M., Hu, Z., & Majumder, E. L.-W. (2024). Co-occurrence of Direct and Indirect Extracellular Electron Transfer Mechanisms during Electroactive Respiration in a Dissimilatory Sulfate Reducing Bacterium. *BioRxiv*, 2024.03.28.587247. <https://doi.org/10.1101/2024.03.28.587247>
- Ichikawa, H., Takagi, T., Uchiyama, K., Higashihara, H., Katada, K., Isozaki, Y., Naito, Y., Yoshida, N., & Yoshikawa, T. (2004). Rotenone, a mitochondrial electron transport inhibitor, ameliorates ischemia-reperfusion-induced intestinal mucosal damage in rats. *Redox report: Communications in Free Radical Research*, 9(6), 313–316. <https://doi.org/10.1179/135100004225006795>
- Islam, S., & Karr, E. (2013). Examination of metal corrosion by *Desulfomicrobium thermophilum*, *Archaeoglobus fulgidus*, and *Methanothermobacter thermautotrophicus*. *BIOS*, 84, 59–64. <https://doi.org/10.1893/0005-3155-84.2.59>
- Jackson, B. E., & McInerney, M. J. (2000). Thiosulfate disproportionation by *Desulfotomaculum thermobenzoicum*. *Applied and environmental*

microbiology, 66(8), 3650–3653. <https://doi.org/10.1128/AEM.66.8.3650-3653.2000>

- Jin, X., Yin, X., Ling, L., Mao, H., Dong, X., Chang, X., Chen, M., & Fang, S. (2023). Adding glucose delays the conversion of ethanol and acetic acid to caproic acid in *Lacrimispora celerecrescens* JSJ-1. *Appl. Microbiol. Biotechnol.* **107**, 1453–1463. <https://doi.org/10.1007/s00253-023-12378-7>
- Joseph, A., George, B., Madhusoodanan, K., & Alex, R. (2015). Current status of sulphur vulcanization and devulcanization chemistry: Process of vulcanization. *Rubber Science*, 28, 82.
- Kang, D. D., Li, F., Kirton, E., Thomas, A., Egan, R., An, H., & Wang, Z. (2019). MetaBAT 2: an adaptive binning algorithm for robust and efficient genome reconstruction from metagenome assemblies. *PeerJ* **7**, e7359. <https://doi.org/10.7717/peerj.7359>
- Kappes, M., Frankel, G., Sridhar, N., & Carranza, R. (2012). Corrosion Behavior of Carbon Steel in Acidified, Thiosulfate-Containing Brines. *Corrosion*, 68, 872–884. <https://doi.org/10.5006/0610>
- Kappes, M., Frankel, G., Sridhar, N., & Carranza, R. (2012). Reaction Paths of Thiosulfate during Corrosion of Carbon Steel in Acidified Brines. *Journal of The Electrochemical Society*, 159, C195. <https://doi.org/10.1149/2.085204jes>
- Kempler, P. A., Boettcher, S. W., & Ardo, S. (2021). Reinvigorating electrochemistry education. *iScience*, 24(5), 102481. <https://doi.org/10.1016/j.isci.2021.102481>

- Khan, M. A. A., Hussain, M., & Djavanroodi, F. (2021). Microbiologically influenced corrosion in oil and gas industries: A review. *International Journal of Corrosion and Scale Inhibition*, *10*, 80–106. <https://doi.org/10.17675/2305-6894-2021-10-1-5>
- Kiani Khouzani, M., Bahrami, A., Hosseini-Abari, A., Khandouzi, M., & Taheri, P. (2019). Microbiologically Influenced Corrosion of a Pipeline in a Petrochemical Plant. *Metals - Open Access Metallurgy Journal*, *9*, 459. <https://doi.org/10.3390/met9040459>
- Kip, N., & van Veen, J. A. (2015). The dual role of microbes in corrosion. *The ISME Journal*, *9*(3), 542–551. <https://doi.org/10.1038/ismej.2014.169>
- Kloos W. E. (1980). Natural populations of the genus *Staphylococcus*. *Ann. Rev. Microbiol.* **34**, 559–592. <https://doi.org/10.1146/annurev.mi.34.100180.003015>
- Klose, S., Bilen, S., Tabatabai, M., & Dick, W. (2011). *Sulfur Cycle Enzymes* (pp. 125–151). <https://doi.org/10.2136/sssabookser9.c7>
- Kokilaramani, S., Al-Ansari, M. M., Rajasekar, A., Al-Khattaf, F. S., Hussain, A., & Govarathanan, M. (2021). Microbial influenced corrosion of processing industry by re-circulating waste water and its control measures - A review. *Chemosphere* **265**, 129075. <https://doi.org/10.1016/j.chemosphere.2020.129075>
- LaButti, K., Mayilraj, S., Clum, A., Lucas, S., Glavina Del Rio, T., Nolan, M., Tice, H., Cheng, J.-F., Pitluck, S., Liolios, K., Ivanova, N., Mavromatis, K., Mikhailova, N., Pati, A., Goodwin, L., Chen, A., Palaniappan, K., Land, M., Hauser, L., ...

- Lapidus, A. (2010). Permanent draft genome sequence of *Dethiosulfovibrio peptidovorans* type strain (SEBR 4207T). *Standards in Genomic Sciences*, 3(1), 85–92. <https://doi.org/10.4056/sigs.1092865>
- Lahme, S., Mand, J., Longwell, J., Smith, R., & Enning, D. (2020). Severe corrosion of carbon steel in oil field produced water can be linked to methanogenic archaea containing a special type of [NiFe] hydrogenase. *BioRxiv*, 2020.07.23.219014. <https://doi.org/10.1101/2020.07.23.219014>
- Laitinen, T. (1999). Thiosulfate pitting corrosion of stainless steels in paper machine environment /. *VTT Publications*.
- Lee, Y.-J., Lee, S.-J., Jeong, H., Kim, H., Ryu, N., Kim, B.-C., Lee, H.-S., Lee, D.-W., & Lee, S. J. (2012). Draft genome sequence of *Bacillus oceanisediminis* 2691. *J. Bacteriol.* **194**, 6351–6352. <https://doi.org/10.1128/JB.01643-12>
- Li, H. (2013) Produced Water Quality Characterization and Prediction for Wattenberg Field. Civil and Environmental Engineering, Colorado State University, Fort Collins.
- Li, S., Wu, J., Wang, Y., Zhang, X., Zhang, W., Zhang, Y., & Shi, Q. (2024). Isolation and characterization of thiols in petroleum using Ag⁺-silica solid phase extraction followed by gas chromatography-mass spectrometry and high-resolution mass spectrometry. *Fuel*, 363, 130946. <https://doi.org/https://doi.org/10.1016/j.fuel.2024.130946>

- Li, Z., Yang, J., Lu, S., Dou, W., & Gu, T. (2023). Impact of *Desulfovibrio ferrophilus* IS5 biocorrosion time on X80 carbon steel mechanical property degradation. *Journal of Materials Research and Technology*, 27, 3777–3787.
<https://doi.org/https://doi.org/10.1016/j.jmrt.2023.10.296>
- Liang, D., Liu, X., Woodard, T. L., Holmes, D. E., Smith, J. A., Nevin, K. P., Feng, Y., & Lovley, D. R. (2021). Extracellular Electron Exchange Capabilities of *Desulfovibrio ferrophilus* and *Desulfopila corrodens*. *Environmental science & technology*, 55(23), 16195–16203. <https://doi.org/10.1021/acs.est.1c04071>
- Little, B. J., & Lee, J. S. (2015). Microbiologically Influenced Corrosion. In *Oil and Gas Pipelines* (pp. 387–398).
<https://doi.org/https://doi.org/10.1002/9781119019213.ch27>
- Little, B. J., Blackwood, D. J., Hinks, J., Lauro, F. M., Marsili, E., Okamoto, A., Rice, S. A., Wade, S. A., & Flemming, H.-C. (2020). Microbially influenced corrosion—Any progress? *Corrosion Science*, 170, 108641.
<https://doi.org/https://doi.org/10.1016/j.corsci.2020.108641>
- Little, B. J., Hinks, J., & Blackwood, D. J. (2020). Microbially influenced corrosion: Towards an interdisciplinary perspective on mechanisms. *International Biodeterioration & Biodegradation*, 154, 105062.
<https://doi.org/https://doi.org/10.1016/j.ibiod.2020.105062>
- Loddeke, M., Schneider, B., Oguri, T., Mehta, I., Xuan, Z., & Reitzer, L. (2017). Anaerobic Cysteine Degradation and Potential Metabolic Coordination in

Salmonella enterica and Escherichia coli. *Journal of Bacteriology*, 199, JB.00117-17. <https://doi.org/10.1128/JB.00117-17>

Lyles, C. N., Le, H. M., Beasley, W. H., McInerney, M. J., & Suflita, J. M. (2014). Anaerobic hydrocarbon and fatty acid metabolism by syntrophic bacteria and their impact on carbon steel corrosion. *Front. Microbiol.* **5**, 114. <https://doi.org/10.3389/fmicb.2014.00114>

Machuca, L. L., Lepkova, K., & Petroski, A. (2017). Corrosion of carbon steel in the presence of oilfield deposit and thiosulphate-reducing bacteria in CO₂ environment. *Corrosion Science*, 129, 16–25. <https://doi.org/10.1016/J.CORSCI.2017.09.011>

Madirisha, M., Hack, R., & van der Meer, F. (2022). The role of organic acid metabolites in geo-energy pipeline corrosion in a sulfate reducing bacteria environment. *Heliyon* **8**, e09420. <https://doi.org/10.1016/j.heliyon.2022.e09420>

Marcus, P., & Protopopoff, E. (1997). Thermodynamics of thiosulfate reduction on surfaces of iron, nickel and chromium in water at 25 and 300 °C. *Corrosion Science*, 39(9), 1741–1752. [https://doi.org/https://doi.org/10.1016/S0010-938X\(97\)00079-6](https://doi.org/https://doi.org/10.1016/S0010-938X(97)00079-6)

Martin, G., Sharma, S., Ryan, W., Srinivasan, N. K., & Senko, J. M. (2021). Identification of microbiological activities in wet flue gas desulfurization systems. *Front. Microbiol.* **12**, 675628. <https://www.frontiersin.org/articles/10.3389/fmicb.2021.675628>

- Maskari, N., Almobarak, M., Saeedi, A., & Xie, Q. (2020). Influence of pH on acidic oil-brine-carbonate adhesion using atomic force microscopy. *Energy Fuel*. **34**, 13570-13758. <https://doi.org/10.1021/acs.energyfuels.0c02494>
- Matei, A., Puscas, C., Patrascu, I., Lehene, M., Ziebro, J., Scurtu, F., Baia, M., Porumb, D., Totos, R., & Silaghi-Dumitrescu, R. (2020). On the Stability of Glutaraldehyde in Biocide Compositions. *International journal of molecular sciences*, *21*(9), 3372. <https://doi.org/10.3390/ijms21093372>
- McDonald, D., Price, M.N., Goodrich, J., Nawrocki, E.P., DeSantis, T.Z., Probst, A., Anderson, G. L., Night, R., Hugenholtz, P. (2012). An improved Greengenes taxonomy with explicit ranks for ecological and evolutionary analyses of bacteria and archaea. *ISME J*. **6**, 610–618.
- Menzel, P., Ng, K. L., & Krogh, A. (2016). Fast and sensitive taxonomic classification for metagenomics with Kaiju. *Nat. Comm.* **7**, 11257. <https://doi.org/10.1038/ncomms11257>
- Meyer, B., Kuehl, J. V., Price, M. N., Ray, J., Deutschbauer, A. M., Arkin, A. P., & Stahl, D. A. (2014). The energy-conserving electron transfer system used by *Desulfovibrio alaskensis* strain G20 during pyruvate fermentation involves reduction of endogenously formed fumarate and cytoplasmic and membrane-bound complexes, Hdr-Flox and Rnf. *Environmental microbiology*, *16*(11), 3463–3486. <https://doi.org/10.1111/1462-2920.12405>
- Miller, R. B., Ghadimi, H., Chinthala, S. P., Sadek, A., Crouch, A. L., Floyd, J. G., Stevenson, B. S., Crookes-Goodson, W., Senko, J. M., & Monty, C. N. (2023).

Evaluation of microbial corrosion in biofuel storage tanks using split-chamber zero resistance ammetry. *Journal of Applied Electrochemistry*, 53(6), 1269–1277.
<https://doi.org/10.1007/s10800-022-01834-3>

Miller, R. B., Sadek, A., Crouch, A. L., Floyd, J. G., Drake, C. A., Stevenson, B. S., Crookes-Goodson, W., Monty, C. N., & Senko, J. M. (2020). Novel Mechanism of Microbially Induced Carbon Steel Corrosion at an Aqueous/Non-aqueous Interface. *Industrial and Engineering Chemistry Research*, 59(35), 15784–15790.
<https://doi.org/10.1021/acs.iecr.0c02497>

Miller, R. B., Sadek, A., Rodriguez, A., Iannuzzi, M., Gai, C., Senko, J. M., & Monty, C. N. (2016). Use of an Electrochemical Split Cell Technique to Evaluate the Influence of *Shewanella oneidensis* Activities on Corrosion of Carbon Steel. *PLOS ONE*, 11(1), e0147899. <https://doi.org/10.1371/journal.pone.0147899>

Miller, R., Lawson, K., Sadek, A., Monty, C., & Senko, J. (2018). Uniform and Pitting Corrosion of Carbon Steel by *Shewanella oneidensis* MR-1 under Nitrate-Reducing Conditions. *Applied and Environmental Microbiology*, 84, AEM.00790-18. <https://doi.org/10.1128/AEM.00790-18>

Montville, T. J., Parris, N., & Conway, L. K. (1985). Influence of pH on organic acid production by *Clostridium sporogenes* in test tube and fermenter cultures. *Applied and Environmental Microbiology*, 49(4), 733–736.
<https://doi.org/10.1128/aem.49.4.733-736.1985>

- Neria-González, I., Wang, E. T., Ramírez, F., Romero, J. M., and Hernández- Rodríguez, C. (2006). Characterization of bacterial community associated to biofilms of corroded oil pipelines from the southeast of Mexico. *Anaerobe* **12**, 122–133. doi: 10.1016/j.anaerobe.2006.02.00
- Nurk, S., Meleshko, D., Korobeynikov, A., & Pevzner, P. A. (2017). metaSPAdes: a new versatile metagenomic assembler. *Genome Res.* **27**, 824–834. <https://doi.org/10.1101/gr.213959.116>
- Nurk, S., Meleshko, D., Korobeynikov, A., & Pevzner, P. A. (2017). metaSPAdes: a new versatile metagenomic assembler. *Genome Res.* **27**, 824–834. <https://doi.org/10.1101/gr.213959.116>
- Oguri, T., Schneider, B., & Reitzer, L. (2012). Cysteine catabolism and cysteine desulfhydrase (CdsH/STM0458) in *Salmonella enterica* serovar typhimurium. *Journal of bacteriology*, *194*(16), 4366–4376. <https://doi.org/10.1128/JB.00729-12>
- Ohkuma, M., Noda, s, Hattori, S., Iida, T., Yuki, M., Starns, D., Inoue, J.-I., Darby, A., & Hongoh, Y. (2015). Acetogenesis from H₂ plus CO₂ and nitrogen fixation by an endosymbiotic spirochete of a termite-gut cellulolytic protist. *Proceedings of the National Academy of Sciences of the United States of America*, *112*. <https://doi.org/10.1073/pnas.1423979112>
- Ondov, B. D., Bergman, N. H., & Phillippy, A. M. (2011). Interactive metagenomic visualization in a Web browser. *BMC Bioinformatics* **12**, 385. <https://doi.org/10.1186/1471-2105-12-385>

- Ozay, E. I., Sherman, H. L., Mello, V., Trombley, G., Lerman, A., Tew, G. N., Yadava, N., & Minter, L. M. (2018). Rotenone Treatment Reveals a Role for Electron Transport Complex I in the Subcellular Localization of Key Transcriptional Regulators During T Helper Cell Differentiation. *Frontiers in immunology*, *9*, 1284. <https://doi.org/10.3389/fimmu.2018.01284>
- Pal, M. K., & Lavanya, M. (2022). Microbial Influenced Corrosion: Understanding Bioadhesion and Biofilm Formation. *Journal of Bio- and Tribo-Corrosion*, *8*(3), 76. <https://doi.org/10.1007/s40735-022-00677-x>
- Parks, D. H., Chuvochina, M., Chaumeil, P. A., Rinke, C., Mussig, A. J., & Hugenholtz, P. (2020). A complete domain-to-species taxonomy for Bacteria and Archaea. *Nat. Biotechnol.* **38**, 1079–1086. <https://doi.org/10.1038/s41587-020-0501-8>
- Parks, D. H., Imelfort, M., Skennerton, C. T., Hugenholtz, P., & Tyson, G. W. (2015). CheckM: assessing the quality of microbial genomes recovered from isolates, single cells, and metagenomes. *Genome Res.* **25**, 1043–1055. <https://doi.org/10.1101/gr.186072.114>
- Parks, D., Chuvochina, M., Waite, D., Rinke, C., Skarchewski, A., Chaumeil, P.-A., Hugenholtz, P. (2018). A standardized bacterial taxonomy based on genome phylogeny substantially revises the tree of life. *Nat. Biotechnol.* **36**, 996–1004. <https://doi.org/10.1038/nbt.4229>
- Parshina, S., Kleerebezem, R., Sanz, J., Lettinga, G., Nozhevnikova, A., Kostrikina, N., Lysenko, A., & Stams, A. (2003). *Soehngenia saccharolytica* gen. nov., sp. nov and *Clostridium amygdalinum* sp. nov., two novel anaerobic, benzaldehyde-

converting bacteria. *Int. J. System. Evol. Microbiol.* **53**, 1791–1799.

<https://doi.org/10.1099/ijs.0.02668-0>

Pedregosa, F., Varoquaux, G., Gramfort, A., Michel, V., Thirion, B., Grisel, O., Blondel, M., Prettenhofer, P., Weiss, R., Dubourg, V., Vanderplas, I., Passos, A., Cournapeau, D., Brucher, M., Perrot, M., & Duchesnay, E. (2011). Scikit-learn: machine learning in python. *J. Machine Learn. Res.* **12**, 2825-2830.

Pedroza-Dávila, U., Uribe-Alvarez, C., Morales-García, L., Espinoza-Simón, E., Méndez-Romero, O., Muhlia-Almazán, A., Chiquete-Félix, N., & Uribe-Carvajal, S. (2020). Metabolism, ATP production and biofilm generation by *Staphylococcus epidermidis* in either respiratory or fermentative conditions. *AMB Expr.* **10**, 31.
<https://doi.org/10.1186/s13568-020-00966-z>

Philips, J. (2020). Extracellular Electron Uptake by Acetogenic Bacteria: Does H₂ Consumption Favor the H₂ Evolution Reaction on a Cathode or Metallic Iron? In *Frontiers in Microbiology* (Vol. 10).
<https://www.frontiersin.org/article/10.3389/fmicb.2019.02997>

Piulle, L., Morelli, X., Gallice, P., Lojou, E., Barbier, P., Czjzek, M., Bianco, P., Guerlesquin, F., & Hatchikian, E. C. (2005). The Type I / Type II Cytochrome c₃ Complex: An Electron Transfer Link in the Hydrogen-Sulfate Reduction Pathway. *Journal of Molecular Biology*, *354*(1), 73–90.
<https://doi.org/https://doi.org/10.1016/j.jmb.2005.09.036>

- Plugge, C., Zhang, W., Scholten, J., & Stams, A. (2011). Metabolic Flexibility of Sulfate-Reducing Bacteria. In *Frontiers in Microbiology* (Vol. 2, p. 81).
<https://www.frontiersin.org/article/10.3389/fmicb.2011.00081>
- Prjibelski, A., Antipov, D., Meleshko, D., Lapidus, A., & Korobeynikov, A. (2020). Using SPAdes de novo assembler. *Curr. Protocol Bioinform.* **70**, e102.
<https://doi.org/10.1002/cpbi.102>
- Prussin, A. J., 2nd, & Marr, L. C. (2015). Sources of airborne microorganisms in the built environment. *Microbiome* **3**, 78. <https://doi.org/10.1186/s40168-015-0144-z>
- Qian, Z., Tianwei, H., Mackey, H. R., van Loosdrecht, M. C. M., & Guanghao, C. (2019). Recent advances in dissimilatory sulfate reduction: From metabolic study to application. *Water Research*, *150*, 162–181.
<https://doi.org/https://doi.org/10.1016/j.watres.2018.11.018>
- Rücker, C., Mahmoud, W. M. M., Schwartz, D., & Kümmerer, K. (2018). Biodegradation tests of mercaptocarboxylic acids, their esters, related divalent sulfur compounds and mercaptans. *Environmental Science and Pollution Research*, *25*(19), 18393–18411. <https://doi.org/10.1007/s11356-018-1812-x>
- Sánchez-Andrea, I., Guedes, I. A., Hornung, B., Boeren, S., Lawson, C. E., Sousa, D. Z., Bar-Even, A., Claassens, N. J., & Stams, A. J. M. (2020). The reductive glycine pathway allows autotrophic growth of *Desulfovibrio desulfuricans*. *Nature communications*, *11*(1), 5090. <https://doi.org/10.1038/s41467-020-18906-7>

- Sanchez-Rosario, R., & Hildenbrand, Z. L. (2022). Produced water treatment and valorization: A techno-economical review. *Energies* **15**, en15134619.
<https://doi.org/10.3390/en15134619>
- Sehmi, S. K., Allan, E., MacRobert, A. J., & Parkin, I. (2016). The bactericidal activity of glutaraldehyde-impregnated polyurethane. *Microbiology Open*, *5*(5), 891–897.
<https://doi.org/10.1002/mbo3.378>
- Shi, Q., & Wu, J. (2021). Review on Sulfur Compounds in Petroleum and Its Products: State-of-the-Art and Perspectives. *Energy & Fuels*, *35*(18), 14445–14461.
<https://doi.org/10.1021/acs.energyfuels.1c02229>
- Shin, J., Song, Y., Kang, S., Jin, S., Lee, J. K., Kim, D. R., Cho, S., Müller, V., & Cho, B. K. (2021). Genome-Scale Analysis of *Acetobacterium woodii* Identifies Translational Regulation of Acetogenesis. *mSystems*, *6*(4), e0069621.
<https://doi.org/10.1128/mSystems.00696-21>
- Silva Campos, M. D. R., Blawert, C., Scharnagl, N., Störmer, M., & Zheludkevich, M. L. (2022). Cathodic Protection of Mild Steel Using Aluminium-Based Alloys. *Materials (Basel, Switzerland)*, *15*(4), 1301.
<https://doi.org/10.3390/ma15041301>
- Sivakanesan, R., & Dawes, E. A. (1980). Anaerobic glucose and serine metabolism in *Staphylococcus epidermidis*. *J. Gen. Microbiol.* **118**, 143–157.
<https://doi.org/10.1099/00221287-118-1-143>
- Stams, A. J. M., & Hansen, T. A. (1984). Fermentation of glutamate and other compounds by *Acidaminobacter hydrogeniformans* gen. nov. sp. nov., an

- obligate anaerobe isolated from black mud. Studies with pure cultures and mixed cultures with sulfate-reducing and methanogenic bacteria. *Archives of Microbiology*, 137(4), 329–337. <https://doi.org/10.1007/BF00410730>
- Steudel, R. and Steudel, Y. (2006), Interaction of Zinc Oxide Clusters with Molecules Related to the Sulfur Vulcanization of Polyolefins (“Rubber”). *Chemistry – A European Journal*, 12: 8589-8602. <https://doi.org/10.1002/chem.200600700>
- Stoffels, L., Krehenbrink, M., Berks, B., & Uden, G. (2012). Thiosulfate Reduction in *Salmonella enterica* Is Driven by the Proton Motive Force. *Journal of Bacteriology*, 194, 475–485. <https://doi.org/10.1128/JB.06014-11>
- Suflita, J. M., Phelps, T. J., & Little, B. (2008). Carbon dioxide corrosion and acetate: A hypothesis on the influence of microorganisms. *Corrosion*, 64(11), 854–859. <https://doi.org/10.5006/1.3279919>
- Takagi, H., & Ohtsu, I. (2017). L-Cysteine Metabolism and Fermentation in Microorganisms. *Advances in biochemical engineering/biotechnology*, 159, 129–151. https://doi.org/10.1007/10_2016_29
- Tang, K. (2020). Chemical Diversity and Biochemical Transformation of Biogenic Organic Sulfur in the Ocean. In *Frontiers in Marine Science* (Vol. 7). <https://www.frontiersin.org/articles/10.3389/fmars.2020.00068>
- Tang, K.-H., Tang, Y. J., & Blankenship, R. E. (2011). Carbon Metabolic Pathways in Phototrophic Bacteria and Their Broader Evolutionary Implications. *Frontiers in Microbiology*, 2.

<https://www.frontiersin.org/journals/microbiology/articles/10.3389/fmicb.2011.00>

165

Tanner, R. S., (2007). Cultivation of bacteria and fungi. *In*: Hurst, C. J., Crawford, R. J., Garland, J. L., Lipson, D. A., Mills, A. L., Stetzenbach, L. D. (eds) *Manual of Environmental Microbiology*, 3rd ed. ASM Press, Washington, DC. Pp 69-76.

Tasaki, M., Kamagata, Y., Nakamura, K., Okamura, K., & Minami, K. (1993).

Acetogenesis from pyruvate by *Desulfotomaculum thermobenzoicum* and differences in pyruvate metabolism among three sulfate-reducing bacteria in the absence of sulfate. *FEMS Microbiology Letters*, 106(3), 259–263.

<https://doi.org/10.1111/j.1574-6968.1993.tb05973.x>

Thapaliya, D., Hellwig, E. J., Kadariya, J., Grenier, D., Jefferson, A. J., Dalman, M., Kennedy, K., DiPerna, M., Orihill, A., Taha, M., & Smith, T. C. (2017).

Prevalence and characterization of *Staphylococcus aureus* and methicillin-resistant *Staphylococcus aureus* on public recreational beaches in Northeast Ohio. *GeoHealth*, 1, 320–332. <https://doi.org/10.1002/2017GH000106>

Thyne, G., & Brady, P. (2016). Evaluation of formation water chemistry and scale prediction: Bakken Shale. *Appl. Geochem.* 75.

<https://doi.org/10.1016/j.apgeochem.2016.10.015>

Tran, P. Q., Bachand, S. C., Hotvedt, J. C., Kieft, K., McDaniel, E. A., McMahon, K. D., & Anantharaman, K. (2022). Microbial cysteine degradation is a source of

hydrogen sulfide in oxic freshwater lakes. *BioRxiv*, 2021.11.30.467465.

<https://doi.org/10.1101/2021.11.30.467465>

Tsurumaru, H., Ito, N., Mori, K., Wakai, S., Uchiyama, T., Iino, T., Hosoyama, A., Ataku, H., Nishijima, K., Mise, M., Shimizu, A., Harada, T., Horikawa, H., Ichikawa, N., Sekigawa, T., Jinno, K., Tanikawa, S., Yamazaki, J., Sasaki, K., ... Harayama, S. (2018). An extracellular [NiFe] hydrogenase mediating iron corrosion is encoded in a genetically unstable genomic island in *Methanococcus maripaludis*. *Scientific Reports*, 8(1), 15149. <https://doi.org/10.1038/s41598-018-33541-5>

Ueki T. (2021). Cytochromes in Extracellular Electron Transfer in *Geobacter*. *Applied and environmental microbiology*, 87(10), e03109-20.
<https://doi.org/10.1128/AEM.03109-20>

Videla, H. A. (2002). Prevention and control of biocorrosion. *International Biodeterioration & Biodegradation*, 49(4), 259–270.
[https://doi.org/https://doi.org/10.1016/S0964-8305\(02\)00053-7](https://doi.org/https://doi.org/10.1016/S0964-8305(02)00053-7)

Vigneron, A., Alsop, E., Chambers, B., Lomans, B., Head, I., & Tsesmetzis, N. (2016). Complementary Microorganisms in Highly Corrosive Biofilms from an Offshore Oil Production Facility. *Applied and Environmental Microbiology*, 82, AEM.03842-15. <https://doi.org/10.1128/AEM.03842-15>

- Vigneron, A., Head, I. M., & Tsesmetzis, N. (2018). Damage to offshore production facilities by corrosive microbial biofilms. *Appl. Microbiol. Biotechnol.* **102**, 2525–2533. <https://doi.org/10.1007/s00253-018-8808-9>
- Walsh, B. J. C., & Giedroc, D. P. (2020). H₂S and reactive sulfur signaling at the host-bacterial pathogen interface. *Journal of Biological Chemistry*, *295*(38), 13150–13168. <https://doi.org/https://doi.org/10.1074/jbc.REV120.011304>
- Wang, D., Kijikla, P., Mohamed, M. E., Saleh, M. A., Kumseranee, S., Punpruk, S., & Gu, T. (2021). Aggressive corrosion of carbon steel by *Desulfovibrio ferrophilus* IS5 biofilm was further accelerated by riboflavin. *Bioelectrochemistry*, *142*, 107920. <https://doi.org/https://doi.org/10.1016/j.bioelechem.2021.107920>
- Won, J. H., Park, S., Hong, S., Son, S., & Yu, J. W. (2015). Rotenone-induced Impairment of Mitochondrial Electron Transport Chain Confers a Selective Priming Signal for NLRP3 Inflammasome Activation. *The Journal of biological chemistry*, *290*(45), 27425–27437. <https://doi.org/10.1074/jbc.M115.667063>
- Wu, K., Dai, L., Tu, B., Zhang, X., Zhang, H., Deng, Y., Lawson, P., & Cheng, L. (2019). *Gudongella oleilytica* gen. nov., sp. nov., an aerotolerant bacterium isolated from Shengli oilfield and validation of family Tissierellaceae. *International Journal of Systematic and Evolutionary Microbiology*, *70*. <https://doi.org/10.1099/ijsem.0.003854>
- Wu, Y. W., Tang, Y. H., Tringe, S. G., Simmons, B. A., & Singer, S. W. (2014). MaxBin: an automated binning method to recover individual genomes from

- metagenomes using an expectation-maximization algorithm. *Microbiome*, 2, 26.
<https://doi.org/10.1186/2049-2618-2-26>
- Xu, D., Gu, T., & Lovley, D. R. (2023). Microbially mediated metal corrosion. *Nature Reviews Microbiology*, 21(11), 705–718. <https://doi.org/10.1038/s41579-023-00920-3>
- Xu, D., Li, Y., & Gu, T. (2016). Mechanistic modeling of biocorrosion caused by biofilms of sulfate reducing bacteria and acid producing bacteria. *Bioelectrochemistry* **110**, 52–58. <https://doi.org/10.1016/j.bioelechem.2016.03.003>
- Xu, D., Li, Y., Song, F., & Gu, T. (2013). Laboratory investigation of microbiologically influenced corrosion of C1018 carbon steel by nitrate reducing bacterium *Bacillus licheniformis*. *Corrosion Science*, 77, 385–390.
<https://doi.org/https://doi.org/10.1016/j.corsci.2013.07.044>
- Yokota, A., & Ikeda, M. (2017). Amino Acid Fermentation. *Amino Acid Fermentation*.
- Zane, G., Wall, J., & De Leon, K. (2020). Novel Mode of Molybdate Inhibition of *Desulfovibrio vulgaris* Hildenborough. *Frontiers in Microbiology*, 11.
<https://doi.org/10.3389/fmicb.2020.610455>
- Zhang, J., Liu, R., Xi, S., Cai, R., Zhang, X., & Sun, C. (2020). A novel bacterial thiosulfate oxidation pathway provides a new clue about the formation of zero-valent sulfur in deep sea. *The ISME Journal*, 14(9), 2261–2274.
<https://doi.org/10.1038/s41396-020-0684-5>

- Zhang, J., Wang, J., Fang, C., Song, F., Xin, Y., Qu, L., & Ding, K. (2010). *Bacillus oceanisediminis* sp. nov., isolated from marine sediment. *Int. J. System. Evol. Microbiol.* **60**, 2924–2929. <https://doi.org/10.1099/ijs.0.019851-0>
- Zhang, P., Huang, S., Zhang, N., Kan, A.T., & Tomson, M. (2019). Automated analytical method to determine solution alkalinity of oilfield brine in the presence of weak organic acids. *Ind. Eng. Chem Res.* **58**, 4667-4673
- Zhang, P., Xu, D., Li, Y., Yang, K., & Gu, T. (2015). Electron mediators accelerate the microbiologically influenced corrosion of 304 stainless steel by the *Desulfovibrio vulgaris* biofilm. *Bioelectrochemistry*, *101*, 14–21.
<https://doi.org/https://doi.org/10.1016/j.bioelechem.2014.06>.

APPENDIX

Below is a citation and summary of the Chinthala paper referenced above.

Chinthala, S. P., Sadek, A., Davis, J., Senko, J. M., & Monty, C. N. (2023). Real-time electrochemical monitoring of the progress of sulfate reducing bacterially-induced corrosion of carbon steel. *Corrosion* 4415. <https://doi.org/10.5006/4415>

Summary:

Microbiologically influenced corrosion (MIC) poses a significant challenge in the oil and gas industry, particularly due to the activity of sulfate-reducing bacteria (SRB). A sulfate-reducing enrichment culture was obtained from a natural gas transmission line and tested using split chamber-zero resistance ammetry (SC-ZRA) to monitor corrosion dynamics. Carbon steel electrodes were immersed in synthetic gas field brine in opposing chambers, with one chamber inoculated with SRB and the other remaining uninoculated to simulate heterogeneous metal surface coverage. Initial positive current between the electrodes in the presence of an organic electron donor (lactate) suggested an initial priming phase by planktonic SRB. This transitioned to negative current, indicating that the cathodic corrosion reaction was occurring on the electrode exposed to SRB. Similar

negative current patterns were observed in both lactate-free incubations and uninoculated controls with sulfide, supporting SRB-induced corrosion mechanisms. These findings, corroborated by SRB metabolic activities and mass loss data, underscore the dynamic nature of SRB-mediated corrosion and highlight the potential of real-time electrochemical monitoring for MIC detection.

Personal Contributions

As part of my personal contributions to the paper, I was responsible for the growth and characterization of a sulfate-reducing bacterial (SRB) culture derived from a natural gas pipeline pigging sludge sample, utilizing 16S rRNA sequencing for identification. I also played a significant role in running split chamber-zero resistance ammetry (SC-ZRA) experiments, including conducting post-experimental analyses and interpreting the results. Additionally, I performed batch experiments to further explore the microbial activities and corrosion mechanisms associated with the SRB culture, enhancing our understanding of microbiologically influenced corrosion in the context of natural gas pipelines.